Divergent receptor proteins confer responses to different karrikins in two ephemeral weeds

Yueming Kelly Sun[1,2], Adrian Scaffidi[1], Jiaren Yao[1], Kim Melville[1], Steven M Smith[3,4], Gavin R Flematti[1] and Mark T Waters[1,2,5]

1. School of Molecular Sciences, The University of Western Australia, 35 Stirling Hwy, Perth, WA 6009, Australia
2. Australian Research Council Centre of Excellence in Plant Energy Biology, The University of Western Australia, 35 Stirling Hwy, Perth, WA 6009, Australia
3. School of Natural Sciences, The University of Tasmania, Hobart, TAS 7000, Australia
4. Institute of Genetics and Developmental Biology, Chinese Academy of Sciences, 1 West Beichen Road, Beijing 100101, PR China.
5. Author for correspondence: mark.waters@uwa.edu.au

Word count (Abstract, main text and methods): 5143 words

ABSTRACT

Wildfires can encourage the establishment of invasive plants by releasing potent germination stimulants, such as karrikins. Seed germination of *Brassica tournefortii*, a noxious weed of Mediterranean climates, is strongly stimulated by KAR_1, which is the most abundant karrikin produced from burning vegetation. In contrast, the closely-related yet non-fire-associated ephemeral *Arabidopsis thaliana* responds preferentially to the less abundant KAR_2. The α/β-hydrolase KARRIKIN INSENSITIVE2 (KAI2) is the putative karrikin receptor identified in *Arabidopsis*. Here we show that *B. tournefortii* differentially expresses three *KAI2* homologues, and the most highly-expressed homologue is sufficient to confer enhanced responses to KAR_1 relative to KAR_2 when expressed in *Arabidopsis*. We further identify two variant amino acid residues near the KAI2 active site that explain the ligand selectivity. Our results suggest that duplication and diversification of KAI2 proteins could confer upon weedy ephemerals differential responses to chemical cues produced by environmental disturbance, including fire. (146 words)

INTRODUCTION

Environmental disturbance promotes the establishment of invasive species, posing a potent threat to global biodiversity. Changing wildfire regimes, such as increasing frequency of fires, is one of the most relevant disturbance factors contributing to elevated invasion threat[1]. Wildfires create germination opportunities in part by releasing seed germination stimulants, such as karrikins, from burning vegetation[2, 3]. Karrikins comprise a family of butenolides with six known members. In samples of smoke water generated by burning grass straw, KAR_1 is the most abundant karrikin, while KAR_2 is six times less abundant[4]. These two analogues differ only by the presence of a methyl group on the butenolide ring in KAR_1, which is absent in KAR_2 (Supplementary Fig. 1a). Invasive plant species that are responsive to karrikins could utilise natural and human-induced fires to facilitate their establishment[5, 6].

Brassica tournefortii (Brassicaceae; Sahara mustard) is native to northern Africa and the Middle East, but is an invasive weed that blights many ecosystems with a Mediterranean climate and chaparral-type vegetation that are prone to wildfires in North America, Australia and South Africa. *B. tournefortii* seed can persist in the soil for many seasons, undergoing wet-dry cycling that can influence dormancy and contribute to boom-bust cycles that outcompete native

species[7, 8]. *B. tournefortii* plants may radically alter fire frequency and intensity by influencing fuel profiles[9, 10], further exacerbating the impact of fire on susceptible native ecosystems. In addition, seed of *B. tournefortii* is particularly responsive to smoke-derived karrikins, and shows a positive germination response to KAR_1 in the nanomolar range[11]. Accordingly, *B. tournefortii* is particularly well positioned to invade areas disturbed by fire events[12, 13].

The putative karrikin receptor KARRIKIN INSENSITIVE 2 (KAI2) was identified in *Arabidopsis thaliana*, a weedy ephemeral that originated in Eurasia but is now widely distributed throughout the northern hemisphere[14, 15, 16]. Arabidopsis is not known to colonise fire-prone habitats, but nevertheless seeds germinate in response to karrikins in the micromolar range[17]. Unlike most smoke-responsive species that respond more readily to KAR_1[18, 19], Arabidopsis responds preferentially to the less abundant analogue KAR_2[17]. KAI2 is an evolutionarily ancient α/β-hydrolase and a paralogue of DWARF14 (D14), the receptor for strigolactones[20, 21]. Karrikins and strigolactones are chemically similar by virtue of a butenolide moiety that is necessary for bioactivity[22, 23]. KAI2 and D14 have dual functions as both enzyme and receptor, but the functional significance of the enzymatic activity remains contested[24, 25, 26, 27, 28]. Furthermore, the basis for ligand specificity by these two highly congruent proteins remains essentially unknown.

Orthologues of *KAI2* are ubiquitous in land plants, and are normally present as a single gene copy within an ancient and highly conserved "eu-KAI2" clade[29]. There is growing evidence that, beyond its ability to mediate karrikin responses, KAI2 has a core ancestral role in perceiving an endogenous karrikin-like ligand ("KL") that regulates seed germination, seedling development, leaf shape and cuticle development[30, 31, 32]. Since its divergence from the Arabidopsis lineage, the tribe Brassiceae, which includes the genus *Brassica*, underwent a whole genome triplication event 24–29 million years ago[33, 34, 35]. This process might have allowed additional KAI2 copies to gain altered ligand specificity, potentially enhancing perception of environmental signals such as karrikins from smoke. Here, we report that two KAI2 homologues expressed in *B. tournefortii* show distinct preferences for different karrikins. We take advantage of the relatively recent genome triplication event in the Brassiceae to identify two amino acids that are sufficient to explain these karrikin preferences and confirm this by mutagenesis. Beyond demonstrating the potential ecological significance of diversity among KAI2 homologues, our findings also reveal active site regions critical for ligand selectivity in the broader family of KAI2–D14 receptor-enzymes.

78 # RESULTS

79 ## *B. tournefortii* is most sensitive to KAR_1

80 To characterise the karrikin response of *B. tournefortii*, we performed multiple physiological
81 and molecular assays comparing KAR_1 activity with that of KAR_2. First, germination of *B.*
82 *tournefortii* seeds was consistently more responsive to KAR_1 than KAR_2 at 10 nM, 100 nM and
83 1 μM (Fig. 1a and Supplementary Fig. 1b-d). Second, homologues of two karrikin-responsive
84 transcripts, *D14-LIKE2* (*BtDLK2*) and *SALT TOLERANCE HOMOLOG7* (*BtSTH7*), required ten-
85 fold higher concentrations of KAR_2 (1 μM) compared with KAR_1 (100 nM) to reach equivalent
86 levels (Fig. 1b). These observed differences in seed response are not due to differential karrikin
87 uptake, since both KAR_1 and KAR_2 were taken up from solution at similar rates by *B. tournefortii*
88 seeds during imbibition, as was also true for Arabidopsis seeds (Supplementary Fig. 1e-f).
89 Besides promoting germination of primary dormant seeds, karrikins also inhibited hypocotyl
90 elongation in *B. tournefortii* seedlings, as is the case in Arabidopsis; again, KAR_1 showed a
91 stronger effect than KAR_2 (Fig. 1c-d). Expression of *BtDLK2* transcripts in seedlings was also
92 more responsive to KAR_1 than KAR_2 at a given concentration (Fig. 1e). Therefore, we conclude
93 that *B. tournefortii* is more sensitive to KAR_1 than to KAR_2, a ligand preference that is a feature
94 of many karrikin-responsive species from ecosystems prone to fires[18, 19].

95 ## Two *B. tournefortii* KAI2 homologues are functional in Arabidopsis

96 To establish whether there are multiple *KAI2* homologues present in *B. tournefortii*, we
97 examined transcriptomes from seeds and seedlings. Three putative *KAI2* homologues were
98 identified (*BtKAI2a*, *BtKAI2b*, and *BtKAI2c*; Fig. 2a; Supplementary Fig. 2 and 3). *BtKAI2a*
99 grouped with *AtKAI2* and those of other Brassicaceae within a single clade, whereas *BtKAI2b*
100 and *BtKAI2c* grouped within a clade unique to *Brassica*. This phylogenetic pattern implies that
101 *BtKAI2a* is the ancestral copy of *KAI2*, whereas *BtKAI2b* and *BtKAI2c* presumably arose more
102 recently via genome triplication during the evolution of *Brassica*. All three *BtKAI2* transcripts
103 were expressed in *B. tournefortii* seeds, but only *BtKAI2a* and *BtKAI2b* could be detected in
104 seedlings (Fig. 2b). Across seed and seedlings, *BtKAI2b* transcripts were the most abundant of
105 the three, but there were no consistent effects on any of the transcripts by treatment with 1 μM
106 KAR_1. We also identified two *BtD14* homologues, at least one of which is functionally
107 orthologous to *AtD14* (Supplementary Figs. 2 and 4).

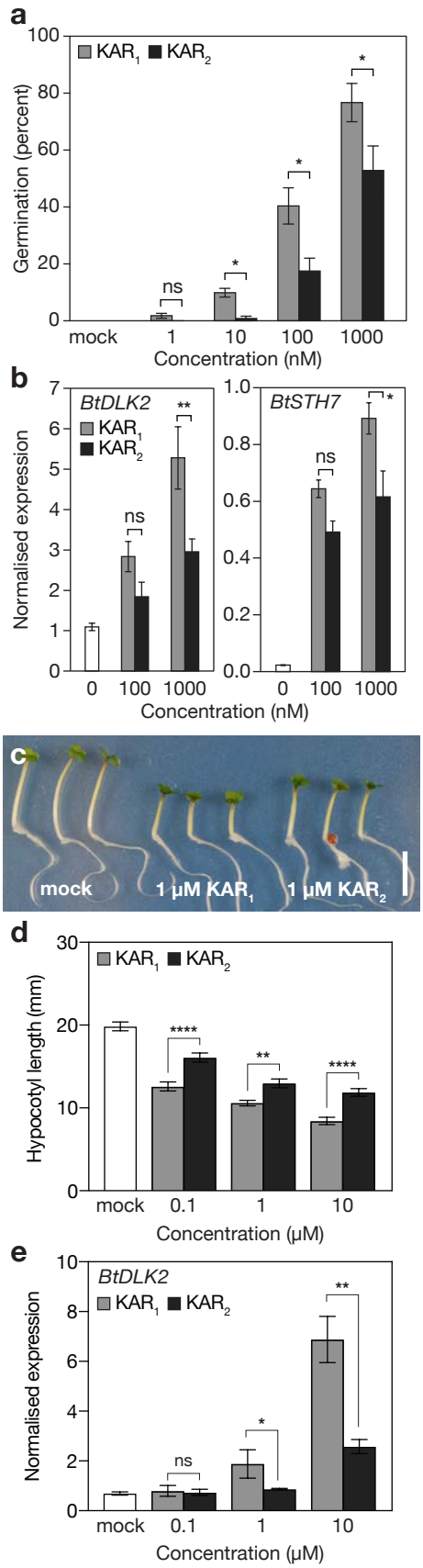

Figure 1. *Brassica tournefortii* is most sensitive to KAR_1, the major karrikin analogue isolated from plant-derived smoke

a, Germination responses of *B. tournefortii* seed to KAR_1 and KAR_2. Data are cumulative germination after 11 days (means ± SE; *n* = 3 biological replicates per treatment, ≥35 seeds per replicate). **b**, Levels of karrikin-responsive transcripts *BtDLK2* and *BtSTH7* in *B. tournefortii* seed. Seed were imbibed for 24 hours in the dark supplemented with KAR_1 and KAR_2. Transcripts were normalised to *BtCACS* reference transcripts. Data are means ± SE, *n* = 3 biological replicates, ≥50 seeds per replicate. **c**, **d**, Hypocotyl elongation responses of *B. tournefortii* seedlings treated with KAR_1 and KAR_2 and grown for four days under continuous red light. Data are means ± 95% CI of *n* = 18 to 24 seedlings. Scale bar: 10 mm. **e**, Levels of *BtDLK2* transcripts in *B. tournefortii* seedlings grown under the same conditions as for d. Data are means ± SE, *n* = 3 biological replicates, ≥20 seedlings per replicate. In all panels, asterisks denote significance levels

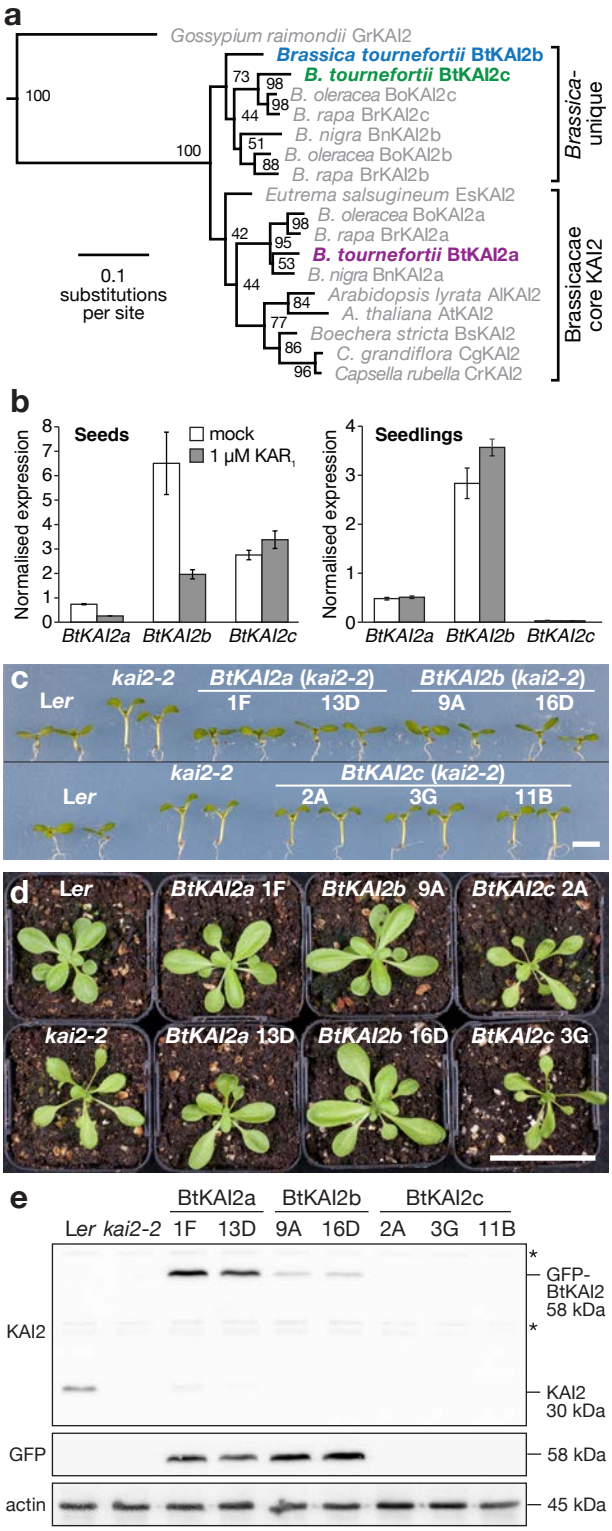

Figure 2. Two differentially expressed *B. tournefortii* KAI2 homologues are functional in Arabidopsis
a, Maximum likelihood phylogeny of KAI2 homologues in the Brassicaceae, based on nucleotide data. Node values represent bootstrap support from 100 replicates. A *KAI2* sequence from *Gossypium raimondii* (Malvaceae) serves as an outgroup. Tree shown is a subset of a larger phylogeny in Supplementary Figure 2. **b**, Transcript levels of the three *BtKAI2* homologues in *B. tournefortii* seed imbibed for 24 h (left) and four-day-old *B. tournefortii* seedlings (right) treated with or without 1 μM KAR_1 for 24 h. Data are means ± SE, n = 3 biological replicates. **c, d,** Seedling and rosette phenotypes of two independent transgenic lines of Arabidopsis homozygous for *KAI2pro:GFP-BtKAI2* transgenes. Scale bars: 5 mm (**c**); 50 mm (**d**).**e**, Immunoblots of soluble proteins challenged with antibodies against KAI2 (upper panel), GFP (middle panel) or actin (lower panel). Non-specific bands are marked with asterisks. Protein was isolated from pools of approximately fifty 7-day-old seedlings.

108 We performed transgenic complementation of the Arabidopsis *kai2-2* null mutant by
109 expressing each of the three isoforms as a GFP fusion protein driven by the Arabidopsis *KAI2*
110 promoter (*KAI2pro*:*GFP-BtKAI2*). Such fusions of GFP with KAI2 proteins have been used
111 previously to analyse KAI2 activity[14, 36, 37]. Both *BtKAI2a* and *BtKAI2b* complemented the
112 seedling and leaf phenotypes of *kai2-2*, whereas *BtKAI2c* did not, despite being expressed at the
113 transcriptional level (Fig. 2c-d and Supplementary Fig. 5a). We could not detect GFP-BtKAI2c
114 protein in three independent transgenic lines, while GFP-BtKAI2a and GFP-BtKAI2b
115 accumulated at consistent levels when detected using an anti-GFP antibody (thereby negating
116 the effects of sequence differences in the anti-KAI2 epitope region; Fig. 2e and Supplementary
117 Fig. 5b). To rule out the possibility that the *GFP-BtKAI2c* transgene is inaccurately expressed in
118 Arabidopsis, we amplified the full-length cDNA from transgenic plant material by RT-PCR,
119 generating a product of the expected size (Supplementary Fig. 6). Two sequenced clones of this
120 RT-PCR product matched the original coding sequence present in the transgene. As such, the
121 *GFP-BtKAI2c* mRNA is processed faithfully in Arabidopsis, and the apparent absence of protein
122 is most likely a result of posttranslational events. Consistent with this interpretation, transient
123 expression in tobacco leaves produced levels of BtKAI2c protein that were considerably lower
124 than for BtKAI2a and BtKAI2b, suggesting that BtKAI2c is poorly expressed in plant cells
125 (Supplementary Fig. 5c). BtKAI2c carries several unique amino acid substitutions, which
126 together may compromise protein folding and stability (Supplementary Fig. 3). Therefore, we
127 conclude that BtKAI2a and BtKAI2b are functionally orthologous to AtKAI2 in regulating plant
128 development, whereas BtKAI2c is an aberrant gene that is potentially non-functional.

129 **BtKAI2a and BtKAI2b show differential ligand specificity**

130 We further characterised the ligand specificity of *BtKAI2* homologues by performing
131 physiological and molecular assays with the transgenic lines. Primary-dormant Arabidopsis
132 seeds homozygous for the transgenes were tested for germination response (Fig. 3a and
133 Supplementary Fig. 7). Germination of *BtKAI2b* transgenic seeds was more responsive to KAR_1
134 than KAR_2 at 1 μM, whereas no significant difference was observed for *BtKAI2a* transgenic
135 seeds. *BtKAI2c* transgenic seeds were insensitive to karrikins. Hypocotyl elongation responses
136 (Fig. 3b) and accumulation patterns of *DLK2* transcripts (Fig. 3c) agreed with the germination
137 response with respect to karrikin preferences. Therefore, and consistent with their relative
138 phylogenetic positions (Fig. 2a), we conclude that *BtKAI2a* has similarity to *AtKAI2* in terms of
139 ligand specificity, whereas *BtKAI2b* has a preference for KAR_1 over KAR_2. As *BtKAI2b* is more
140 highly expressed than *BtKAI2a* in *B. tournefortii* seed and seedlings (Fig. 2b), we suggest that

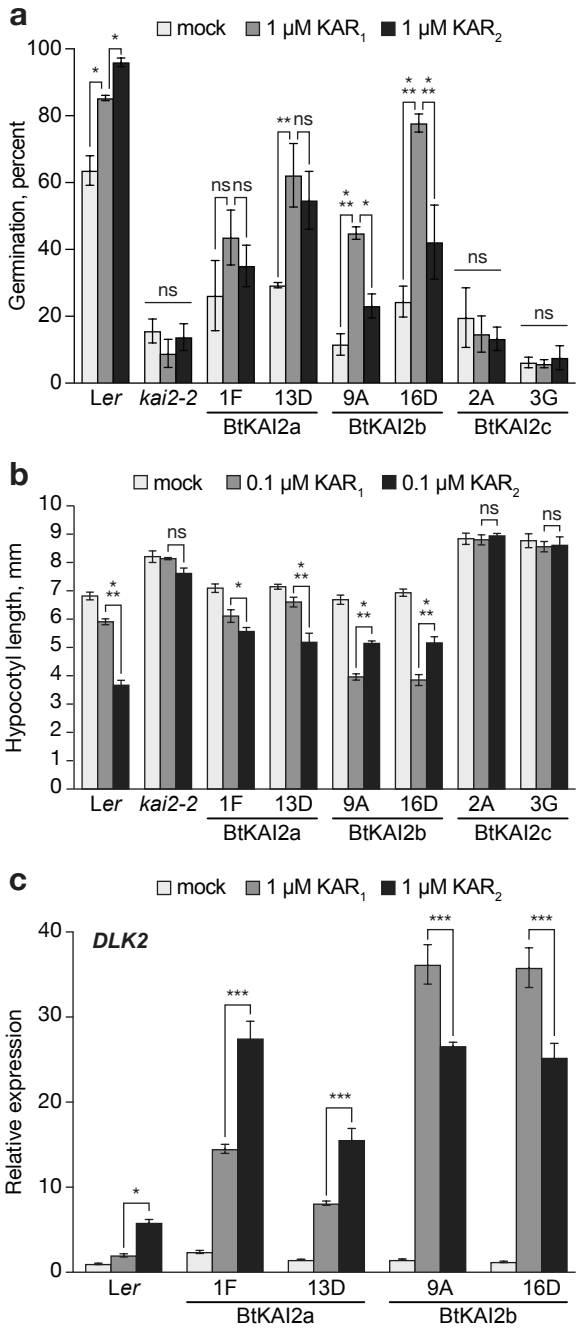

Figure 3. Functional divergence between BtKAI2 homologues

a, Germination responses of primary dormant Arabidopsis seed homozygous for *KAI2pro:GFP-BtKAI2* transgenes in the *kai2-2* background. Germination values were determined 120 h after sowing. Extended germination curves are shown in Supplementary Fig. 6. Data are means ± SE of n = 3 independent seed batches, 75 seed per batch. **b**, Hypocotyl elongation responses of *KAI2pro:GFP-BtKAI2* seedlings treated with KAR_1 or KAR_2. Data are means ± SE of n = 3 biological replicates, 12–18 seedlings per replicate. **c**, Levels of *DLK2* transcripts in 8-day-old *KAI2pro:GFP-BtKAI2* seedlings treated with KAR_1 or KAR_2 for eight hours. Expression was normalised to *CACS* reference transcripts and scaled to the value for mock-treated seedlings within each genotype. Data are means ± SE of n = 3 biological replicates. Pairwise significant differences: * $P < 0.05$ ** $P < 0.01$ *** $P < 0.001$; ns, $P > 0.05$ (two-way ANOVA).

141 the ligand specificity of BtKAI2b accounts for the enhanced KAR_1-responsiveness of this
142 species.

143 ### Positions 98 and 191 account for ligand specificity between BtKAI2a and BtKAI2b

144 To investigate interactions between BtKAI2 homologues and ligands, we performed differential
145 scanning fluorimetry (DSF) assays on purified recombinant proteins (Supplementary Fig. 8).
146 DSF has been used extensively for inferring the interaction of strigolactone-like compounds
147 with D14- and KAI2-related proteins[25, 37, 38, 39, 40, 41]. Racemic GR24 is a widely-used synthetic
148 strigolactone analogue that consists of two enantiomers, of which GR24$^{ent\text{-}5DS}$ is bioactive via
149 AtKAI2[42]. Catalytically inactive D14 and KAI2 variants do not respond to GR24 in DSF,
150 suggesting that the shift in thermal response results from ligand hydrolysis and a
151 corresponding conformational change in the receptor[25, 37, 39]. In DSF assays, AtKAI2 shows a
152 specific response to >100 μM GR24$^{ent\text{-}5DS}$ but, for unclear reasons, no response to karrikins[37].
153 Likewise, we found that both BtKAI2a and BtKAI2b were also unresponsive to karrikins in DSF
154 (Supplementary Fig. 9a). Therefore, we used GR24$^{ent\text{-}5DS}$ as a surrogate substrate in DSF assays
155 to interrogate BtKAI2–ligand interactions.

156 We found that AtKAI2 and BtKAI2a showed similar responses to >100 μM GR24$^{ent\text{-}5DS}$, but the
157 BtKAI2b response was clear at >25 μM (Supplementary Fig. 9b). We then used a lower range of
158 GR24$^{ent\text{-}5DS}$ concentrations (0–50 μM) to determine the threshold for response, which we
159 defined as a statistically significant reduction in the maximal rate of change in fluorescence at
160 the melting temperature of the protein (T_m). Although BtKAI2a showed only a weak and non-
161 significant response at 40 and 50 μM GR24$^{ent\text{-}5DS}$, BtKAI2b responded significantly at 10 μM and
162 above (Fig. 4a). These results suggest that BtKAI2b is more sensitive than BtKAI2a to GR24$^{ent\text{-}}$
163 ^{5DS}, and that BtKAI2a is most like AtKAI2 in this respect.

164 BtKAI2a and BtKAI2b differ in primary amino acid sequence at just 14 positions
165 (Supplementary Fig. 3). We postulated that differences in ligand specificity might be
166 determined by amino acids in the vicinity of the ligand binding pocket. Protein structural
167 homology models revealed only two residues that differ in this region: V98 and V191 in
168 BtKAI2a (Fig. 4b), and L98 and L191 in BtKAI2b (Fig. 4c); the corresponding residues in AtKAI2
169 (Fig. 4d) and AtD14 (Fig. 4e) are valines. Residue 98 is immediately adjacent to the catalytic
170 serine at the base of the pocket. Residue 191 is located internally on αT4 of the lid domain
171 which, in AtD14, is associated with a major rearrangement of protein structure upon ligand
172 binding that reduces the size of the pocket[27]. Homology modelling suggests only subtle

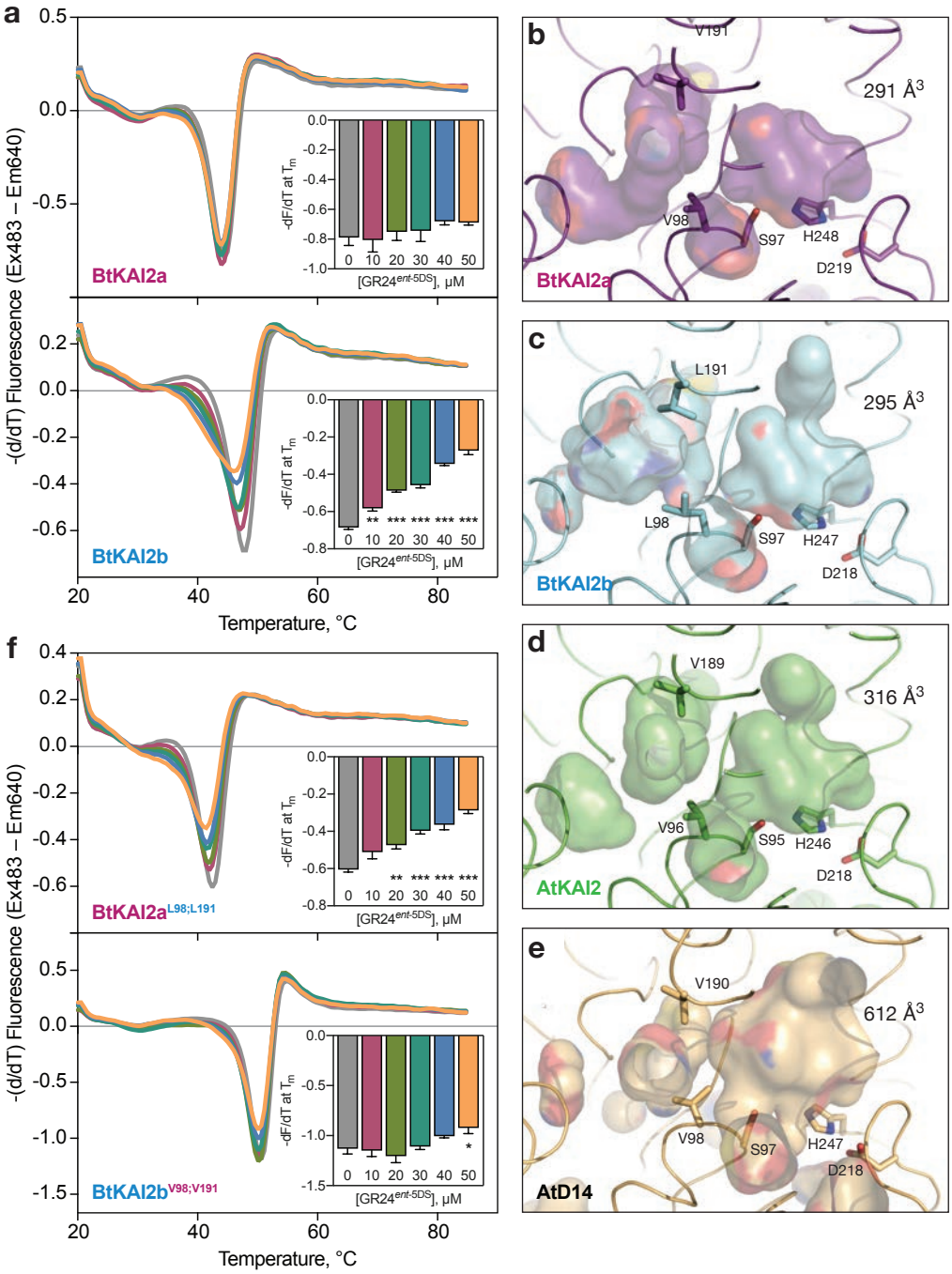

Figure 4. Two residues account for ligand specificity between BtKAI2a and BtKAI2b
a, DSF curves of SUMO-BtKAI2a and SUMO-BtKAI2b fusion proteins treated with 0-50 µM GR24$^{ent\text{-}5DS}$, a KAI2-bioactive ligand. Each curve is the average of three sets of reactions, each comprising four technical replicates. Insets plot the minimum value of –(dF/dT) at the melting point of the protein as determined in the absence of ligand (means ± SE, n = 3). Significant differences from untreated control: * $P < 0.05$ ** $P < 0.01$ *** $P < 0.001$ (ANOVA). **b**, DSF curves of SUMO-BtKAI2a$^{L98;L191}$ and SUMO-BtKAI2b$^{V98;V191}$ fusion proteins treated with 0-50 µM GR24$^{ent\text{-}5DS}$. **c–f**, Solved structure of AtKAI2 (PDB: 3w06, Kagiyama et al 2013), AtD14 (PDB: 4IH4, Zhao et al 2013) and derived homology models of BtKAI2a and BtKAI2b. Coloured surfaces depict internal cavities; values indicate the volumes of the primary ligand-binding cavities, adjacent to the catalytic Ser-His-Asp residues. Also shown is a variable secondary pocket, to the left of the primary pocket in these images.

differences in the size and shape of the primary ligand binding pocket of BtKAI2a and BtKAI2b (Fig. 4b-c). To determine if these residues are pertinent to ligand specificity, we replaced the two valine residues of BtKAI2a with leucine residues, generating the variant BtKAI2a$^{L98;L191}$, and *vice-versa* for BtKAI2b, generating the variant BtKAI2b$^{V98;V191}$ (Supplementary Fig. 8). In DSF assays, we found that exchanging the two residues was sufficient to switch the original responses, such that BtKAI2a$^{L98;L191}$ responded sensitively to GR24$^{ent\text{-}5DS}$, but BtKAI2b$^{V98;V191}$ did not (Fig. 4f).

We reasoned that the most robust method to assess the effect of residues 98 and 191 upon the response to karrikins was to test their function directly *in planta*. We expressed BtKAI2a$^{L98;L191}$ and BtKAI2b$^{V98;V191}$ in the Arabidopsis *kai2-2* null mutant background, and selected two independent homozygous transgenic lines for each, on the basis of protein expression level and segregation ratio (Supplementary Fig. 10). Using two different assays, we found that substitutions between BtKAI2a and BtKAI2b at positions 98 and 191 also reversed karrikin preference in Arabidopsis seedlings (Fig. 5a-b; Supplementary Fig. 11). Most prominently, the clear preference of BtKAI2b for KAR_1 was unambiguously reversed to a preference for KAR_2 in *GFP-BtKAI2b$^{V98;V191}$* transgenics, effectively recapitulating the response of the native BtKAI2a protein. Taken together, these results demonstrate that these two variant residues are sufficient to account for differences in ligand specificity between BtKAI2a and BtKAI2b. Finally, given the importance of these residues, it is notable that the non-functional BtKAI2c carries a highly non-conservative arginine residue at position 98, which might disrupt ligand binding, if not protein folding entirely (Supplementary Fig. 3).

DISCUSSION

The KAI2–D14 family of α/β-hydrolases is characterised by reactivity towards butenolide compounds, including endogenous strigolactones and strigolactone-related compounds, abiotic karrikins derived from burnt vegetation, and synthetic strigolactone analogues with a wide array of functional groups. Direct evidence for a receptor-ligand relationship between karrikins and KAI2 homologues stems from crystallography and *in vitro* binding assays. Two crystal structures of KAR-responsive KAI2 proteins from Arabidopsis and the parasitic plant *Striga hermonthica* reveal largely similar overall protein structure, but surprisingly are non-congruent with respect to KAR_1 binding position and orientation[43, 44]. The affinity of AtKAI2 for KAR_1 is imprecisely defined, with estimates of dissociation coefficients (Kd) ranging from 4.6

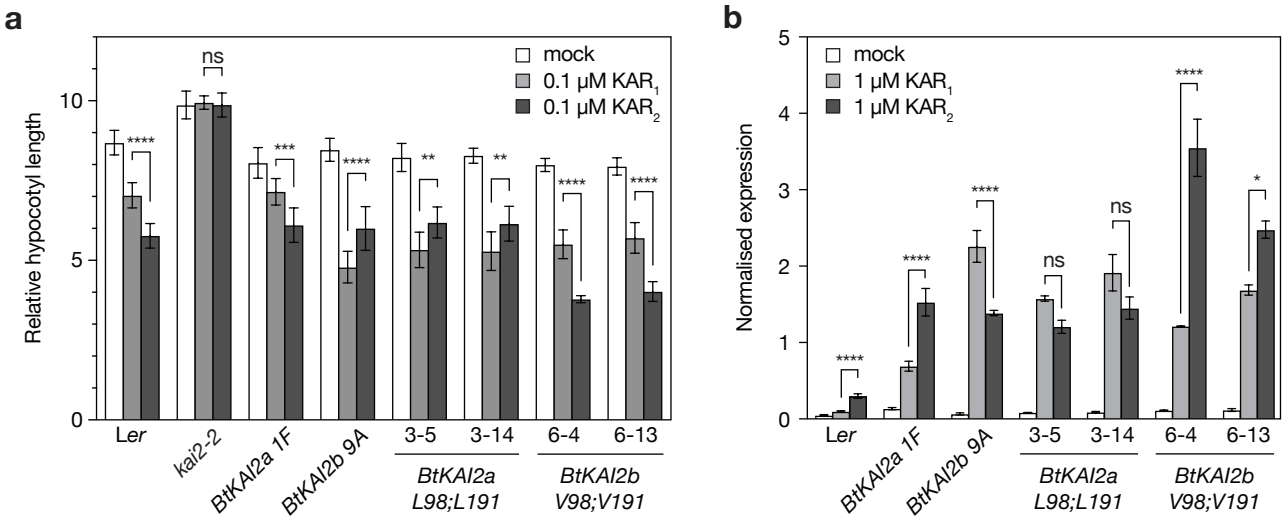

Figure 5. Substitutions between BtKAI2a and BtKAI2b at positions 98 and 191 reverse karrikin preference in transgenic Arabidopsis.

a, Hypocotyl elongation responses to karrikins in two independent transgenic lines homozygous for *GFP-BtKAI2a*$^{L98;L191}$ (3-5, 3-14) and two lines for *GFP-BtKAI2b*$^{V98;V191}$ (6-4, 6-13). Data shown are a summary of three experimental replicates performed on separate occasions, each comprising 20-40 seedlings per genotype/treatment combination. Data for each replicate are shown in Supplementary Figure 10. Error bars are SE, n=3 experimental replicates; each dot corresponds to the mean value derived from each replicate. Asterisks denote significant differences: * P<0.05, ** P<0.01, *** P<0.001, **** P<0.0001 (linear mixed model with experimental replicate as a random effect; specific pairwise comparisons using Tukey's HSD correction).

b, Levels of *DLK2* transcripts in the same transgenic lines treated with 1 μM KAR_1, 1 μM KAR_2, or 0.1% acetone and harvested 8 hours later. Expression was normalised to *CACS* reference transcripts. Data are means ± SE of n=3 pools of 50-100 seedlings treated in parallel. Asterisks denote significant differences as above (two-way ANOVA; specific pairwise comparisons using Tukey's HSD correction).

204 μM[45], to 26 μM[46], to 148 μM[47] using isothermal calorimetry, and 9 μM using fluorescence
205 microdialysis[43]. While variability in affinity estimates can be explained in part by different
206 experimental conditions and techniques, it should also be considered that, depending on the
207 homologue under examination, KAR_1 may not be the optimal ligand. Our data, which benefit
208 from clear and distinct biological responses, provide strong evidence that KAI2 is sufficient to
209 determine ligand specificity, which in turn strengthens the case that KAI2 is the receptor by
210 which karrikins are perceived.

211 Ligand specificity is a key contributor to functional distinction between KAI2–D14 family
212 receptors, and elucidating the molecular mechanisms behind ligand specificity is a significant
213 research challenge. In certain root-parasitic weeds in the Orobanchaceae, substitutions of bulky
214 residues found in AtKAI2 with smaller hydrophobic amino acids that increase the ligand-
215 binding pocket size have likely improved the affinity for host-derived strigolactone ligands, as
216 opposed to the smaller-sized karrikin ligands[48, 49, 50]. Moreover, lid-loop residues that affect the
217 rigidity and size of the ligand entry tunnel determine the ligand selectivity between KAR_1 and
218 *ent*-5-deoxystrigol (a strigolactone analogue with non-natural stereochemistry) among eleven
219 KAI2 homologues in *Physcomitrella patens*[51]. Karrikin and strigolactone compounds also show
220 chemical diversity within themselves, yet ligand discrimination among KAI2–D14 family
221 receptors is not well characterised. Our data demonstrate that, in the case of BtKAI2 proteins,
222 different KAI2 homologues respond differently to highly similar KAR analogues, and that subtle
223 changes in pocket residues likely account for preferences between these ligands. Although the
224 identified residues L98 and L191 do not significantly change the pocket size of BtKAI2b in
225 comparison to BtKAI2a, these residues would make the BtKAI2b pocket more hydrophobic,
226 which is consistent with KAR_1 being more hydrophobic than KAR_2[4]. Therefore, ligand
227 specificity between highly-similar chemical analogues can be achieved through fine-tuning of
228 pocket hydrophobicity. Similarly subtle changes have been reported for the rice gibberellin
229 receptor GID1: changing Ile133 to Leu or Val increases the affinity for GA_{34} relative to the less
230 polar GA_4, which lacks just one hydroxyl group[52]. KAI2–D14 family receptors may also show
231 ligand specificity towards diverse natural strigolactones, resulting in part from multiplicity of
232 biosynthetic enzymes, such as the cytochrome P450 enzymes in the MAX1 family[38, 53, 54] and
233 supplementary enzymes such as LATERAL BRANCHING OXIDOREDUCTASE[55]. Although the
234 functional reasons underlying such strigolactone diversity are still unclear, it is possible that
235 variation among D14 homologues yields varying affinities for different strigolactone
236 analogues[56]. As an increasingly refined picture emerges of the features that determine ligand

237 specificity for KAI2–D14 family receptors, we envision the rational design of synthetic receptor
238 proteins with desirable ligand specificity in the future.

239 Gene duplication is a common feature in plant evolutionary histories as an initial step towards
240 neofunctionalisation[57]. In obligate parasitic weeds, duplication and diversification of *KAI2*
241 genes (also referred to as *HTL* genes) have shifted ligand specificity towards strigolactones[48,
242 49]. Karrikins, as abiotic molecules with limited natural occurrence, are unlikely to be the natural
243 ligand for most KAI2 proteins, which are found throughout land plants. Instead, the
244 evolutionary maintenance of a highly conserved receptor probably reflects the core KAI2
245 function of perceiving an endogenous ligand ("KL") that regulates plant development[30, 31, 32].
246 This core function is presumably retained after gene duplication events through ancestral, non-
247 divergent copies that are under purifying selection[48, 49]. KAI2 diversity may also reflect differing
248 affinity for KL analogues in different species and at different life stages. Our results are
249 consistent with a scenario in which both BtKAI2a and BtKAI2b have retained the core KAI2
250 function of perceiving KL to support plant development, because both copies fully complement
251 the Arabidopsis *kai2* phenotype. However, BtKAI2b has also acquired mutations that alter its
252 ligand specificity, which in turn enhance sensitivity to the more abundant karrikin released
253 after fire. The *BtKAI2b* gene is also more highly expressed than *BtKAI2a* in seeds and seedlings,
254 consistent with an adaptation to post-fire seedling establishment. This diversity among KAI2
255 proteins may provide *B. tournefortii* with a selective advantage in fire-prone environments,
256 assisting its invasive nature.

257 Recent findings indicate that KAI2 is an integrator that also modulates germination in response
258 to other abiotic environmental signals, including temperature and salinity[58]. As seed
259 germination is a critical life stage that contributes to the invasiveness of a species, strategies
260 for weed control will benefit from specific knowledge of KAI2 sequence diversity and
261 expression profiles.

262 METHODS

263 Chemical synthesis

264 Karrikins (KAR_1 and KAR_2), $^{13}[C]_5$-labelled karrikins and GR24 enantiomers ($GR24^{5DS}$ and
265 $GR24^{ent\text{-}5DS}$) were prepared as previously described[59, 60].

266 ## Plant material

267 Arabidopsis *kai2-2* (L*er*) and *Atd14-1* (Col-0) mutants were previously described[15]. Arabidopsis
268 plants were grown on a 6:1:1 mixture of peat-based compost (Seedling Substrate Plus; Bord Na
269 Mona, Newbridge, Ireland), vermiculite and perlite, respectively. Light was provided by wide-
270 spectrum white LED panels emitting 120-150 µmol photons.m^{-2}.s^{-1} with a 16 h light/8 h dark
271 photoperiod, a 22 °C light/16 °C dark temperature cycle, and constant 60% relative humidity.
272 The seeds of *Brassica tournefortii* used in this work were collected in November and December
273 2009 from two sites in Western Australia (Kings Park in Perth, and Merridin)[61]. *Brassica*
274 *tournefortii* seeds were dried to 15% relative humidity for one month prior to storage in air-
275 tight bags at –20 °C.

276 ## Seed germination assays

277 Seed germination assays using Arabidopsis were performed on Phytagel as described
278 previously[42]. *Brassica tournefortii* seeds were sowed in triplicates (35-70 seeds each) on glass
279 microfibre filter paper (Grade 393; Filtech, NSW Australia) held in petri dishes and
280 supplemented with mock or karrikin treatments. Treatments were prepared by diluting
281 acetone (mock) or karrikin stocks (dissolved in acetone) 1:1000 with ultrapure water. Because
282 germination of *B. tournefortii* is inhibited by light[8], the seeds were imbibed in the dark at 22 °C.
283 Numbers of germinated seeds were counted each day until the germination percentages
284 remained unchanged.

285 ## Hypocotyl elongation assays

286 Arabidopsis hypocotyl elongation assays were performed under red light as described
287 previously[15]. For *B. tournefortii*, assays were performed with the following modifications to the
288 Arabidopsis protocol: *B. tournefortii* seeds were sowed in triplicate on glass microfibre filter
289 paper (Filtech) held in petri-dishes supplemented with mock or karrikin treatments. The seeds
290 were imbibed in the dark for 22 h at 24 °C before exposing to continuous red light (5 µmol
291 photons m^{-2} s^{-1}) for 4 days.

292 ## Transcript analysis

293 *Brassica tournefortii* seeds were imbibed on glass fibre filters in the dark at 22 °C as described
294 above. For transcript quantification in *B. tournefortii* seeds, samples were taken at the indicated
295 time points, briefly blot-dried on paper towel, and frozen in liquid nitrogen. For *B. tournefortii*

296 seedlings, two methods were used. For data shown in Fig. 1e, seeds were sowed and seedlings
297 grown in triplicate under identical conditions to those described for hypocotyl elongation
298 assays For data shown in Fig. 2b, seeds were first imbibed for 24 h in the dark, and then
299 transferred to the growth room (~120-150 µmol photons m^{-2} s^{-2} white light, 16 h light/8 h dark,
300 22 °C light/16 °C dark) for three days. A sample of approximately 20 seedlings was then
301 transferred to a 250 mL conical flask containing 50 mL sterile ultrapure water supplemented
302 with 1 µM KAR_1, or an equivalent volume of acetone (0.1% v/v), with three replicate samples
303 per treatment. The flasks were then shaken for 24 h before seedlings were harvested.

304 Arabidopsis seedlings were grown on 0.5× MS agar under growth room conditions (wide-
305 spectrum white LED panels emitting 120-150 µmol photons.m^{-2}.s^{-1} with a 16 h light/8 h dark
306 photoperiod and a 22 °C light/16 °C dark temperature cycle) for seven days. On the seventh
307 day, seedlings were transferred to 3 mL liquid 0.5× MS medium in 12-well culture plates
308 (CORNING Costar 3513) and shaken at 70 rpm for a further 22 h under the same growth room
309 conditions. The medium was then removed by pipette and replaced with fresh medium
310 containing relevant compounds or an equivalent volume (0.1% v/v) acetone. After a further
311 incubation period with shaking (8 h), the seedlings were harvested, blotted dry, and frozen in
312 liquid nitrogen.

313 RNA extraction, DNase treatment, cDNA synthesis and quantitative PCR were conducted as
314 previously described[62]. All oligonucleotides are listed in the Supplementary Table 2.

315 **Cloning and mutagenesis of *Brassica tournefortii KAI2* and *D14* homologues**

316 Full-length *BtKAI2* coding sequences (and unique 3′UTR sequences) were amplified from *B.*
317 *tournefortii* cDNA with Gateway-compatible *attB* sites using the universal forward primer
318 BtKAI2_universal_F and homologue-specific reverse primers RACE_R (BtKAI2a), Contig1_R
319 (BtKAI2b) and Contig5_R (BtKAI2c), before cloning into pDONR207 (Life Technologies). The
320 pDONR207 clones were confirmed by Sanger sequencing and recombined with pKAI2pro-GFP-
321 GW[37] to generate the binary plant expression plasmids pKAI2pro-GFP-BtKAI2a, pKAI2pro-
322 GFP-BtKAI2b and pKAI2pro-GFP-BtKAI2c. For transient expression in tobacco, BtKAI2 coding
323 sequences were transferred via Gateway-mediated recombination into pSKI106, which drives
324 very high expression and encodes an N-terminal 3× *c*-myc tag[63]. The *BtD14a* coding sequence
325 was amplified from cDNA using oligonucleotides BtD14_F and BtD14_R, cloned into pDONR207
326 as above, and transferred into pD14pro-GW[37].

327 The full-length *BtKAI2* coding sequences (excluding 3′UTRs) were amplified from the
328 pDONR207 clones and reconstituted with the pE-SUMO vector by Gibson Assembly to generate
329 the heterologous expression plasmids pE-SUMO-BtKAI2a and pE-SUMO-BtKAI2b. Site-directed
330 mutagenesis generated the heterologous expression plasmids pE-SUMO-BtKAI2a$^{L98;L191}$ and
331 pE-SUMO-BtKAI2b$^{V98;V191}$. For expression of *GFP-BtKAI2a*$^{L98;L191}$ and *GFP-BtKAI2b*$^{V98;V191}$
332 variants in Arabidopsis, site-directed mutagenesis was performed on pDONR207 clones prior
333 to recombination with pKAI2pro-GFP-GW. In both cases, the targeted residues were mutated
334 simultaneously in one PCR product, while the remainder of the plasmid was amplified in a
335 second PCR product. The mutated plasmids were reconstituted by Gibson assembly, and coding
336 regions confirmed by Sanger sequencing.

337 **Plant transformation**

338 Homozygous *kai2-2* plants were transformed by floral dip. Primary transgenic seedlings were
339 selected on sterile 0.5× MS medium supplemented with 20 µg/mL hygromycin B. T_2 lines
340 exhibiting a 3:1 ratio of hygromycin resistant-to-sensitive seedlings were propagated further
341 to identify homozygous lines in the T_3 generation. Experiments were performed from the T_3
342 generation onwards.

343 For transient expression in tobacco, *Agrobacterium* (GV3101) carrying pSKI106 variants was
344 grown in LB medium (25 mL) supplemented with antibiotics and 20 µM acetosyringone until
345 OD_{600} reached 1.0. The bacteria were then harvested by centrifugation (15 min, 5000 × *g*) and
346 resuspended in 10 mM $MgCl_2$, 10 mM MES (pH 5.6) and 100 µM acetosyringone. The optical
347 density was adjusted to 0.4, and the suspension was left standing at 22 °C overnight
348 (approximately 14 h). Leaves of three-week-old *Nicotiana benthamiana* were then infiltrated
349 with a 5-mL syringe, through the abaxial leaf surface. After four days, the leaves were collected
350 and frozen in liquid nitrogen.

351 **Karrikin uptake measurements**

352 Fifteen samples of seed were sowed for each karrikin treatment (five time points, each in
353 triplicate). In each sample, approximately 40 mg of *Brassica tournefortii* seeds were imbibed in
354 3 mL ultrapure water for 24 h in 5-mL tubes. After centrifugation (2 min at 3220 × *g*), excess
355 water was removed by pipette and the volume of residual water (mostly absorbed into the
356 seeds) was calculated by weighing the seeds before and after imbibition. Fresh ultrapure water
357 was added to the fully-imbibed seeds to reach a total volume of 980 µL. Then 20 µL of 100 µM

358 KAR_1 or KAR_2 was added to a final concentration of 2 μM. The seeds were imbibed at 22 °C in
359 darkness. At the indicated time point (0, 2, 4, 8 or 24 h post-treatment), 500 μL of the imbibition
360 solution was removed and combined with 100 ng of either $^{13}[C]_5$-KAR_1 or $^{13}[C]_5$-KAR_2 (100 μL
361 at 1 μg/mL) as an internal standard for quantification purposes. The sample was then extracted
362 once with ethyl acetate (500 μL), and 1 μL of this organic layer was analysed using GC-MS in
363 selective ion monitoring (SIM) mode as previously described[64].

364 The amount of KAR_1 in each sample was calculated by the formula $\frac{A(Ion150)}{A(Ion155)}\times 100$ ng and
365 converted to moles, where *A(Ion150)* indicates the peak area of the ion 150 (KAR_1 to be
366 measured), *A(Ion151)* indicates the peak area of the ion 151 ($^{13}[C]_5$-KAR_1), and 100 ng is the
367 amount of $^{13}[C]_5$-KAR_1 spiked in before the ethyl acetate extraction. Similarly, the amount of
368 KAR_2 in each sample was calculated by the formula $\frac{A(Ion136)}{A(Ion141)}\times 100$ ng and converted to moles.
369 The uptake percentage adjusted to 40 mg of *B. tournefortii* seeds was calculated by the formula:
370 $(1 - \frac{N(x)}{N(0)}) \times \frac{40\ mg}{m\ (seed)}$, where N(0) indicates moles of karrikins at time 0, $N(x)$ indicates moles of
371 karrikins at time point x, and $m(seed)$ indicates the dry weight (mg) of seeds tested in each
372 replicate. For Arabidopsis seeds, the procedure was scaled down for a smaller mass of seeds
373 (20 mg).

374 ## Transcriptome assembly and analysis

375 Twenty milligrams of dry *B. tournefortii* seed was imbibed in water for 24 h and incubated at
376 22 °C in the dark. The seeds were collected by centrifugation, blotted dry, and frozen in liquid
377 nitrogen. A separate sample of seed was sown on glass filter paper, imbibed for 24 h as above,
378 and then incubated for 96 h under continuous red light (20 μmol m^{-2} s^{-1}) with a 22 °C (16 h)/16
379 °C (8h) temperature cycle. A single sample of seedlings (50 mg fresh weight) was harvested and
380 frozen in liquid nitrogen. Total RNA was extracted from both seed and seedling samples using
381 the Spectrum Plant RNA kit (Sigma-Aldrich), including an on-column DNase step. PolyA$^+$ mRNA
382 was purified using oligo(dT) magnetic beads (Illumina), and cDNA libraries for sequencing
383 were generated as described[65]. Sequencing was performed on the Illumina HiSeq 2000
384 platform at the Beijing Genomic Institute, Shenzhen, China. Raw reads were filtered to remove
385 adapters and low-quality reads (those with >5% unknown nucleotides, or those in which
386 greater than 20% of base calls had quality scores ≤10). After filtering, both libraries generated
387 reads with >99.9% of nucleotides attaining Q20 quality score. Transcriptome *de novo* assembly
388 was performed with Trinity[66]. For each library, contigs were assembled into Unigenes;

389 Unigenes from both libraries were then combined, yielding a total of 45,553 predicted coding
390 region sequences with a mean length of 1011 nt. The combined Unigenes were then
391 interrogated for homology to *AtKAI2*, *AtD14*, *AtDLK2*, *AtSTH7* and *AtCACS* using BLASTn
392 searches.

393 **Phylogenetic analysis**

394 *KAI2* and *D14* homologues in *Brassica* species were identified from BLAST searches using
395 Arabidopsis coding sequences as a query. Additional sequences were sampled from an
396 extended phylogenetic analysis[29]. Multiple sequence alignments were performed using MAFFT
397 plugin implemented in Geneious R10 (Biomatters). The alignment was trimmed slightly at the
398 5′ end to remove non-aligned regions of monocot D14 sequences. Maximum likelihood
399 phylogenies were generated using PHYML (GTR +G +I substitution model, combination of NNI
400 and SPR search, and 100 bootstraps). The choice of substitution model was guided by Smart
401 Model Selection in PhyML[67] (http://www.atgc-montpellier.fr/sms). A list of all sequences, and
402 their sources, is provided in Supplementary Table 1.

403 **Protein homology modelling**

404 KAI2 structures were modelled using the SWISS-MODEL server
405 (https://swissmodel.expasy.org) using the alignment mode[68] and the *Arabidopsis thaliana*
406 KAI2 structure 3w06 as a template[45]. Figures of protein structure and homology models were
407 generated using PyMOL v1.3 (Schrödinger LLC). Cavity surfaces were visualised using the
408 "cavities & pockets (culled)" setting in PyMOL and a cavity detection cut-off value of four
409 solvent radii. Cavity volumes were calculated using the CASTp server v3.0[69]
410 (http://sts.bioe.uic.edu/castp) with a probe radius of 1.4Å. Values indicate Connolly's solvent-
411 excluded volumes. Cavities were inspected visually using Chimera v1.12
412 (https://www.cgl.ucsf.edu/chimera/). For both BtKAI2a and BtKAI2b models, CASTp
413 erroneously included surface residues near the primary pocket entrance in the calculation of
414 the pocket volumes. This issue was resolved by the artificial placement of a free alanine residue
415 adjacent to the cavity entrance, as described previously[70].

416 ### Protein expression and purification

417 BtKAI2 proteins were generated as N-terminal 6×HIS-SUMO fusion proteins. All proteins were
418 expressed in BL21 Rosetta DE3 pLysS cells (Novagen) and purified using IMAC as described in
419 detail previously[37].

420 ### Differential scanning fluorimetry

421 DSF was performed in 384-well format and thermal shifts were quantified as described
422 previously[37]. Reactions (10 µL) contained 20 µM protein, 20 mM HEPES pH 7.5, 150 mM NaCl,
423 1.25% (v/v) glycerol, 5× SYPRO Tangerine dye (Molecular Probes) and varying concentrations
424 of ligand that resulted in a final concentration of 5% (v/v) acetone.

425 ### Statistical analysis

426 Data were analysed using one- or two-way ANOVA (α = 0.05, with Tukey's multiple
427 comparisons test). For Figure 5a, in which data from three experimental replicates were
428 combined, data were analysed using a mixed effects model with experimental replicate as a
429 random effect, and genotype and treatment as fixed effects. Prior to ANOVA, germination data
430 were arcsine-transformed, and gene expression data were log-transformed. Tests were
431 implemented in GraphPad Prism version 7.0 or 8.0 (GraphPad Software, graphpad.com).

432 ### Sequence data

433 Sequence data are available at NCBI Genbank under the following accessions: *BtKAI2a*,
434 MG783328; *BtKAI2b*, MG783329; *BtKAI2c*, MG783330; *BtD14a*, MG783331; *BtD14b*,
435 MG783332; *BtDLK2*, MG783333; *BtSTH7*, MK756121; *BtCACS*, MK756122. Raw RNA sequence
436 data from *Brassica tournefortii* seed and seedlings are available in the NCBI SRA database under
437 accession SRP128835.

438 ## REFERENCES

439 1. Early R, *et al.* Global threats from invasive alien species in the twenty-first century and
440 national response capacities. *Nat Commun* **7**, 12485-12485 (2016).

441
442 2. Flematti GR, *et al.* Karrikin and cyanohydrin smoke signals provide clues to new
443 endogenous plant signaling compounds. *Molecular Plant* **6**, 29-37 (2013).

3. Keeley JE, Pausas JG. Evolution of 'smoke' induced seed germination in pyroendemic plants. *South African Journal of Botany* **115**, 251-255 (2018).

4. Flematti GR, Ghisalberti EL, Dixon KW, Trengove RD. Identification of Alkyl Substituted 2 H-Furo[2,3- c]pyran-2-ones as Germination Stimulants Present in Smoke. *Journal of Agricultural and Food Chemistry* **57**, 9475-9480 (2009).

5. Long RL, Stevens JC, Griffiths EM, Adamek M, Powles SB, Merritt DJ. Detecting karrikinolide responses in seeds of the Poaceae. *Australian Journal of Botany* **59**, 610-620 (2011).

6. Milberg P, Lamont BB. Fire enhances weed invasion of roadside vegetation in southwestern Australia. *Biological Conservation* **73**, 45-49 (1995).

7. Bangle DN, Walker LR, Powell EA. Seed germination of the invasive plant *Brassica tournefortii* (Sahara mustard) in the Mojave Desert. In: *Western North American Naturalist* **68**, 334-342 (2008).

8. Long RL*, et al.* Seeds of Brassicaceae weeds have an inherent or inducible response to the germination stimulant karrikinolide. *Annals of Botany* **108**, 933-944 (2011).

9. Brooks ML*, et al.* Effects of Invasive Alien Plants on Fire Regimes. *BioScience* **54**, 677 (2004).

10. Sanders R, Minnich R. Brassica tournefortii. In: *Invasive Plants of California's Wildlands* (eds Bossard CC, Randall JM, Hoshovsky MC). University of California Press (2000).

11. Stevens J, Merritt D, Flematti G, Ghisalberti E, Dixon K. Seed germination of agricultural weeds is promoted by the butenolide 3-methyl-2H-furo[2,3-c]pyran-2-one under laboratory and field conditions. *Plant Soil* **298**, 113-124 (2007).

12. Schiermeier Q. Pall hangs over desert's future as alien weeds fuel wildfires. *Nature* **435**, 724 (2005).

13. Steers RJ. Invasive Plants, Fire Succession, and Restoration of Creosote Bush Scrub in Southern California. UNIVERSITY OF CALIFORNIA RIVERSIDE (2008).

14. Sun X-D, Ni M. HYPOSENSITIVE TO LIGHT, an Alpha/Beta Fold Protein, Acts Downstream of ELONGATED HYPOCOTYL 5 to Regulate Seedling De-Etiolation. *Molecular Plant* **4**, 116-126 (2011).

15. Waters MT, *et al.* Specialisation within the DWARF14 protein family confers distinct responses to karrikins and strigolactones in Arabidopsis. *Development* **139**, 1285-1295 (2012).

16. Durvasula A, *et al.* African genomes illuminate the early history and transition to selfing in *Arabidopsis thaliana*. *Proceedings of the National Academy of Sciences* **114**, 5213-5218 (2017).

17. Nelson DC, *et al.* Karrikins discovered in smoke trigger Arabidopsis seed germination by a mechanism requiring gibberellic acid synthesis and light. *Plant Physiology* **149**, 863-873 (2009).

18. Flematti GR, Goddard-Borger ED, Merritt DJ, Ghisalberti EL, Dixon KW, Trengove RD. Preparation of 2H-furo[2,3-c]pyran-2-one derivatives and evaluation of their germination-promoting activity. *Journal of Agricultural and Food Chemistry* **55**, 2189-2194 (2007).

19. Flematti GR, Ghisalberti EL, Dixon KW, Trengove RD. A compound from smoke that promotes seed germination. *Science* **305**, 977 (2004).

20. Waters MT, Gutjahr C, Bennett T, Nelson DC. Strigolactone Signaling and Evolution. *Annual Review of Plant Biology* **68**, 291-322 (2017).

21. Yao R, Chen L, Xie D. Irreversible strigolactone recognition: a non-canonical mechanism for hormone perception. *Current Opinion in Plant Biology* **45**, 155-161 (2018).

22. Scaffidi A, *et al.* Exploring the molecular mechanism of karrikins and strigolactones. *Bioorganic & Medicinal Chemistry* **22**, 3743-3746 (2012).

23. Zwanenburg B, Pospíšil T. Structure and Activity of Strigolactones: New Plant Hormones with a Rich Future. *Molecular Plant* **6**, 38-62 (2013).

24. de Saint Germain A, *et al.* An histidine covalent receptor and butenolide complex mediates strigolactone perception. *Nature Chemical Biology* **12**, 787-794 (2016).

25. Seto Y, *et al.* Strigolactone perception and deactivation by a hydrolase receptor DWARF14. *Nat Commun* **10**, 191 (2019).

26. Shabek N, Ticchiarelli F, Mao H, Hinds TR, Leyser O, Zheng N. Structural plasticity of D3–D14 ubiquitin ligase in strigolactone signalling. *Nature* **563**, 652-656 (2018).

526
527 27. Yao R, *et al.* DWARF14 is a non-canonical hormone receptor for strigolactone. *Nature*
528 **536**, 469-473 (2016).

529
530 28. Marzec M, Brewer P. Binding or Hydrolysis? How Does the Strigolactone Receptor
531 Work? *Trends in Plant Science*, 10.1016/j.tplants.2019.1005.1001 (2019).

532
533 29. Bythell-Douglas R, *et al.* Evolution of strigolactone receptors by gradual neo-
534 functionalization of KAI2 paralogues. *BMC Biology* **15**, 52 (2017).

535
536 30. Conn CE, Nelson DC. Evidence that KARRIKIN-INSENSITIVE2 (KAI2) Receptors may
537 Perceive an Unknown Signal that is not Karrikin or Strigolactone. *Frontiers in Plant*
538 *Science* **6**, 1219 (2015).

539
540 31. Li W, *et al.* The karrikin receptor KAI2 promotes drought resistance in *Arabidopsis*
541 *thaliana*. *PLoS Genetics* **13**, e1007076 (2017).

542
543 32. Sun YK, Flematti GR, Smith SM, Waters MT. Reporter Gene-Facilitated Detection of
544 Compounds in Arabidopsis Leaf Extracts that Activate the Karrikin Signaling Pathway.
545 *Frontiers in Plant Science* **7**, 1799 (2016).

546
547 33. Liu S, *et al.* The *Brassica oleracea* genome reveals the asymmetrical evolution of
548 polyploid genomes. *Nat Commun* **5**, 3930 (2014).

549
550 34. Lysak MA, Koch MA, Pecinka A, Schubert I. Chromosome triplication found across the
551 tribe Brassiceae. *Genome Res* **15**, 516-525 (2005).

552
553 35. Wang X, *et al.* The genome of the mesopolyploid crop species Brassica rapa. *Nature*
554 *Genetics* **43**, 1035-1039 (2011).

555
556 36. Waters MT, Scaffidi A, Flematti G, Smith SM. Substrate-Induced Degradation of the α/β-
557 Fold Hydrolase KARRIKIN INSENSITIVE2 Requires a Functional Catalytic Triad but Is
558 Independent of MAX2. *Molecular Plant* **8**, 814-817 (2015).

559
560 37. Waters MT, Scaffidi A, Moulin SLY, Sun YK, Flematti GR, Smith SM. A *Selaginella*
561 *moellendorffii* Ortholog of KARRIKIN INSENSITIVE2 Functions in Arabidopsis
562 Development but Cannot Mediate Responses to Karrikins or Strigolactones. *Plant Cell*
563 **27**, 1925-1944 (2015).

564

565 38. Abe S, *et al.* Carlactone is converted to carlactonoic acid by MAX1 in Arabidopsis and its
566 methyl ester can directly interact with AtD14 in vitro. *Proceedings of the National*
567 *Academy of Sciences of the United States of America* **111**, 18084-18089 (2014).

568
569 39. Hamiaux C, *et al.* DAD2 Is an α/β Hydrolase Likely to Be Involved in the Perception of
570 the Plant Branching Hormone, Strigolactone. *Current Biology* **22**, 2032-2036 (2012).

571
572 40. Hamiaux C, *et al.* Inhibition of strigolactone receptors by N-phenylanthranilic acid
573 derivatives: structural and functional insights. *Journal of Biological Chemistry*, (2018).

574
575 41. Végh A, *et al.* Comprehensive Analysis of DWARF14-LIKE2 (DLK2) Reveals Its
576 Functional Divergence from Strigolactone-Related Paralogs. *Frontiers in Plant Science* **8**,
577 (2017).

578
579 42. Scaffidi A, *et al.* Strigolactone hormones and their stereoisomers signal through two
580 related receptor proteins to induce different physiological responses in Arabidopsis.
581 *Plant Physiology* **165**, 1221-1232 (2014).

582
583 43. Guo Y, Zheng Z, La Clair JJ, Chory J, Noel JP. Smoke-derived karrikin perception by the
584 α/β-hydrolase KAI2 from Arabidopsis. *Proceedings of the National Academy of Sciences*
585 *of the United States of America* **110**, 8284-8289 (2013).

586
587 44. Xu Y, *et al.* Structural basis of unique ligand specificity of KAI2-like protein from parasitic
588 weed Striga hermonthica. *Scientific Reports* **6**, 31386 (2016).

589
590 45. Kagiyama M, *et al.* Structures of D14 and D14L in the strigolactone and karrikin signaling
591 pathways. *Genes to Cells* **18**, 147-160 (2013).

592
593 46. Toh S, Holbrook-Smith D, Stokes ME, Tsuchiya Y, McCourt P. Detection of parasitic plant
594 suicide germination compounds using a high-throughput Arabidopsis HTL/KAI2
595 strigolactone perception system. *Chem Commun* **21**, 988-998 (2014).

596
597 47. Lee I, *et al.* A missense allele of KARRIKIN-INSENSITIVE2 impairs ligand-binding and
598 downstream signaling in Arabidopsis thaliana. *Journal of Experimental Botany* **69**, 3609-
599 3623 (2018).

600
601 48. Conn CE, *et al.* Convergent evolution of strigolactone perception enabled host detection
602 in parasitic plants. *Science* **349**, 540-543 (2015).

603
604 49. Toh S, *et al.* Structure-function analysis identifies highly sensitive strigolactone
605 receptors in Striga. *Science* **350**, 203-207 (2015).

606
607 50. Xu Y, *et al.* Structural analysis of HTL and D14 proteins reveals the basis for ligand
608 selectivity in Striga. *Nat Commun* **9**, 3947 (2018).

609
610 51. Bürger M, *et al.* Structural Basis of Karrikin and Non-natural Strigolactone Perception in
611 Physcomitrella patens. *Cell Reports* **26**, 855-865.e855 (2019).

612
613 52. Shimada A, *et al.* Structural basis for gibberellin recognition by its receptor GID1. *Nature*
614 **456**, 520 (2008).

615
616 53. Zhang Y, *et al.* Rice cytochrome P450 MAX1 homologs catalyze distinct steps in
617 strigolactone biosynthesis. *Nature Chemical Biology* **10**, 1028-1033 (2014).

618
619 54. Challis RJ, Hepworth J, Mouchel C, Waites R, Leyser O. A Role for MORE AXILLARY
620 GROWTH1 (MAX1) in Evolutionary Diversity in Strigolactone Signaling Upstream of
621 MAX2. *Plant Physiology* **161**, 1885-1902 (2013).

622
623 55. Brewer PB, *et al. LATERAL BRANCHING OXIDOREDUCTASE* acts in the final stages of
624 strigolactone biosynthesis in *Arabidopsis*. *Proceedings of the National Academy of*
625 *Sciences* **113**, 6301-6306 (2016).

626
627 56. Yoneyama K, *et al.* Which are the major players, canonical or non-canonical
628 strigolactones? *Journal of Experimental Botany* **69**, 2231-2239 (2018).

629
630 57. Panchy N, Lehti-Shiu MD, Shiu S-H. Evolution of gene duplication in plants. *Plant*
631 *Physiology* **171**, 2294-2316 (2016).

632
633 58. Wang L, Waters MT, Smith SM. Karrikin-KAI2 signalling provides Arabidopsis seeds with
634 tolerance to abiotic stress and inhibits germination under conditions unfavourable for
635 seedling establishment. *New Phytologist* **219**, 605-618 (2018).

636
637 59. Goddard-Borger ED, Ghisalberti EL, Stick RV. Synthesis of the germination stimulant 3-
638 methyl-2H-furo[2,3-c]pyran-2-one and analogous compounds from carbohydrates.
639 *European Journal of Organic Chemistry*, 3925-3934 (2007).

640
641 60. Mangnus E, Vanvliet LA, Vadenput D, Zwanenburg B. Structural modifications of strigol
642 analogs - influence of the B and C rings on the bioactivity of the germination stimulant
643 GR24. *Journal of Agricultural and Food Chemistry* **40**, 1222-1229 (1992).

644

645 61. Gorecki MJ, Long RL, Flematti GR, Stevens JC. Parental environment changes the
646 dormancy state and karrikinolide response of Brassica tournefortii seeds. *Annals of*
647 *Botany*, (2012).

648
649 62. Waters MT, Smith SM. KAI2- and MAX2-mediated responses to karrikins and
650 strigolactones are largely independent of HY5 in Arabidopsis seedlings. *Molecular Plant*
651 **6**, 63-75 (2013).

652
653 63. Kagale S*, et al.* TMV-Gate vectors: gateway compatible tobacco mosaic virus based
654 expression vectors for functional analysis of proteins. *Scientific Reports* **2**, 874 (2012).

655
656 64. Flematti GR, Scaffidi A, Dixon KW, Smith SM, Ghisalberti EL. Production of the seed
657 germination stimulant karrikinolide from combustion of simple carbohydrates. *Journal*
658 *of Agricultural and Food Chemistry* **59**, 1195-1198 (2011).

659
660 65. Liang C, Liu X, Yiu S-M, Lim BL. De novo assembly and characterization of *Camelina sativa*
661 transcriptome by paired-end sequencing. *BMC Genomics* **14**, 146 (2013).

662
663 66. Grabherr MG*, et al.* Full-length transcriptome assembly from RNA-Seq data without a
664 reference genome. *Nature Biotechnology* **29**, 644-652 (2011).

665
666 67. Lefort V, Longueville J-E, Gascuel O. SMS: Smart Model Selection in PhyML. *Molecular*
667 *Biology and Evolution* **34**, 2422-2424 (2017).

668
669 68. Bordoli L, Kiefer F, Arnold K, Benkert P, Battey J, Schwede T. Protein structure homology
670 modeling using SWISS-MODEL workspace. *Nature Protocols* **4**, 1-13 (2009).

671
672 69. Dundas J, Ouyang Z, Tseng J, Binkowski A, Turpaz Y, Liang J. CASTp: computed atlas of
673 surface topography of proteins with structural and topographical mapping of
674 functionally annotated residues. *Nucleic Acids Research* **34**, W116-W118 (2006).

675
676 70. Lopez-Obando M*, et al.* Structural modelling and transcriptional responses highlight a
677 clade of PpKAI2-LIKE genes as candidate receptors for strigolactones in Physcomitrella
678 patens. *Planta* **243**, 1441-1453 (2016).

679

680 ## ACKNOWLEDGEMENTS

681 This work was supported by funding from the Australian Research Council (DP130103646
682 to SMS and GRF; DP140104567 to SMS; FT150100162 to MTW, DP160102888 to GRF and

683 MTW). Y.K.S was recipient of a Research Training Program Scholarship from the Australian
684 Government. We thank Dr Rowena Long for the original provision of *B. tournefortii* seeds, Dr
685 Rohan Bythell-Douglas for advice on homology modelling, and Mr Yongjie Meng with assistance
686 with RNA extractions. We are grateful to Dr Kevin Rozwadowski (Agriculture and Agri-Food
687 Canada) for the provision of pSKI106.

688 CONTRIBUTIONS

689 Y.K.S., S.M.S., G.R.F. and M.T.W. conceived and designed the research; Y.K.S., A.S., J.Y., K.M. and
690 M.T.W. performed the experiments; Y.K.S. and M.T.W. analysed the data; Y.K.S., S.M.S. and
691 M.T.W. wrote the manuscript.

692 SUPPLEMENTARY INFORMATION

693 **Supplementary Figure 1** Germination of *Brassica tournefortii* seed treated with karrikins

694 **Supplementary Figure 2** Extended phylogeny of eu-KAI2 and D14 proteins in angiosperms

695 **Supplementary Figure 3** Alignment of Brassica KAI2 sequences

696 **Supplementary Figure 4** BtD14a is functionally homologous to AtD14

697 **Supplementary Figure 5** Expression of BtKAI2 homologues in Arabidopsis and tobacco

698 **Supplementary Figure 6** The *GFP-BtKAI2c* transgene is faithfully transcribed in Arabidopsis

699 **Supplementary Figure 7** Germination profiles of transgenic Arabidopsis seeds expressing
700 BtKAI2 homologues

701 **Supplementary Figure 8** SDS-PAGE of SUMO-BtKAI2 fusion proteins used for DSF

702 **Supplementary Figure 9** BtKAI2a and BtKAI2b do not respond to karrikins in DSF assays

703 **Supplementary Figure 10** Stable transgenic expression of BtKAI2 valine–leucine exchange
704 proteins in Arabidopsis

705 **Supplementary Figure 11** Three experimental replicates of hypocotyl elongation assays with
706 BtKAI2 Arabidopsis transgenics

707 **Supplementary Table 1** List of sequences identified in this study

708 **Supplementary Table 2** List of oligonucleotides

709 FIGURE LEGENDS

710 **Figure 1. *Brassica tournefortii* is highly sensitive to KAR_1, the major karrikin analogue**
711 **isolated from plant-derived smoke**

712 **a,** Germination responses of *B. tournefortii* seed to KAR_1 and KAR_2. Data are cumulative
713 germination after 11 days (mean ± SE; n = 3 biological replicates per treatment, ≥35 seeds per
714 replicate). **b**, Levels of karrikin-responsive transcripts *BtDLK2* and *BtSTH7* in *B. tournefortii*
715 seed. Seed were imbibed for 24 hours in the dark supplemented with KAR_1 and KAR_2.
716 Transcripts were normalised to *BtCACS* reference transcripts. Data are means ± SE, n = 3
717 biological replicates, ≥50 seeds per replicate. **c**, **d**, Hypocotyl elongation responses of *B.*
718 *tournefortii* seedlings treated with KAR_1 and KAR_2 and grown for four days under continuous
719 red light. Data are means ± 95% CI of n = 18 to 24 seedlings. Scale bar: 10 mm. **e**, Levels of
720 *BtDLK2* transcripts in *B. tournefortii* seedlings grown under the same conditions as for **d**. Data
721 are means ± SE, n = 3 biological replicates, ≥20 seedlings per replicate. In all panels, asterisks
722 denote significance levels (ANOVA) between indicated conditions: * P<0.05; ** P<0.01; ***
723 P<0.001; **** P<0.0001.

724 **Figure 2. Two differentially expressed *B. tournefortii KAI2* homologues are functional in**
725 ***Arabidopsis***

726 **a**, Maximum likelihood phylogeny of KAI2 homologues in the Brassicaceae, based on nucleotide
727 data. Node values represent bootstrap support from 100 replicates. A eu-KAI2 sequence from
728 *Gossypium raimondii* (Malvaceae) serves as an outgroup. Tree shown is a subset of a larger
729 phylogeny in Supplementary Fig. 2. **b**, Transcript levels of the three *BtKAI2* homologues in *B.*
730 *tournefortii* seeds imbibed for 24 h (left) and four-day-old seedlings (right) treated with or
731 without 1 μM KAR_1 for 24 h. **c**, **d**, Seedling and rosette phenotypes of two independent
732 transgenic lines of Arabidopsis homozygous for *KAI2pro:GFP-BtKAI2* transgenes. Scale bars: 5
733 mm (**c**); 50 mm (**d**). **e**, Immunoblots of soluble proteins challenged with antibodies against KAI2
734 (upper panel), GFP (middle panel) or actin (lower panel). Non-specific bands are marked with
735 asterisks. Protein was isolated from pools of approximately fifty 7-day-old seedlings.

736

737 **Figure 3. Functional divergence between BtKAI2 homologues**

738 **a**, Germination responses of primary dormant *Arabidopsis* seed homozygous for *KAI2pro:GFP-*
739 *BtKAI2* transgenes in the *kai2-2* background. Germination values were determined 120 h after
740 sowing. Extended germination curves are shown in Supplementary Fig. 7. Data are means ± SE,
741 n = 3 independent seed batches, 75 seed per batch. **b**, Hypocotyl elongation responses of
742 *KAI2pro:GFP-BtKAI2* seedlings treated with KAR_1 or KAR_2. Data are means ± SE of n = 3
743 biological replicates, 12–18 seedlings per replicate. **c**, Levels of *DLK2* transcripts in 8-day-old
744 *KAI2pro:GFP-BtKAI2* seedlings treated with KAR_1 or KAR_2 for eight hours. Expression was
745 normalised to *CACS* reference transcripts and scaled to the value for mock-treated seedlings
746 within each genotype. Data are means ± SE of n = 3 biological replicates. Pairwise significant
747 differences: * $P < 0.05$ ** $P < 0.01$ *** $P < 0.001$; ns, $P > 0.05$ (ANOVA).

748 **Figure 4. Two residues account for ligand specificity between BtKAI2a and BtKAI2b**

749 **a**, DSF curves of SUMO-BtKAI2a and SUMO-BtKAI2b fusion proteins treated with 0-50 μM
750 $GR24^{ent\text{-}5DS}$, a KAI2-bioactive ligand. Each curve is the average of three sets of reactions, each
751 comprising four technical replicates. Insets plot the minimum value of –(dF/dT) at the melting
752 point of the protein as determined in the absence of ligand (means ± SE, n = 3). Significant
753 differences from untreated control: * $P < 0.05$ ** $P < 0.01$ *** $P < 0.001$ (ANOVA). **b–e**, Homology
754 models of BtKAI2a (b) and BtKAI2b (c), and solved structures of AtKAI2 (d, PDB: 3w06) and
755 AtD14 (e, PDB: 4IH4). Coloured surfaces depict internal cavities; values indicate the volumes of
756 the primary ligand-binding cavities, adjacent to the catalytic Ser-His-Asp residues. Also shown
757 is a variable secondary pocket, to the left of the primary pocket in these images. **f**, DSF curves
758 of SUMO-BtKAI2a$^{L98;L191}$ and SUMO-BtKAI2b $^{V98;V191}$ fusion proteins treated with 0-50 μM
759 $GR24^{ent\text{-}5DS}$.

760 **Figure 5. Substitutions between BtKAI2a and BtKAI2b at positions 98 and 191 reverse**
761 **karrikin preference in transgenic Arabidopsis.**

762 **a**, Hypocotyl elongation responses to karrikins in two independent transgenic lines
763 homozygous for *GFP-BtKAI2a*$^{L98;L191}$ (3-5, 3-14) and two lines for *GFP-BtKAI2b*$^{V98;V191}$ (6-4, 6-
764 13). Data shown are a summary of three experimental replicates performed on separate
765 occasions, each comprising 20-40 seedlings per genotype/treatment combination. Data for
766 each replicate are shown in Supplementary Figure 10. Error bars are SE, n=3 experimental
767 replicates; each dot corresponds to the mean value derived from each replicate. Asterisks
768 denote significant differences: * P<0.05, ** P<0.01, *** P<0.001, **** P<0.0001 (linear mixed
769 model with experimental replicate as a random effect; specific pairwise comparisons using

770 Tukey's HSD correction). **b**, Levels of *DLK2* transcripts in the same transgenic lines treated with
771 1 μM KAR_1, 1 μM KAR_2, or 0.1% acetone and harvested 8 hours later. Expression was
772 normalised to *CACS* reference transcripts. Data are means ± SE of n=3 pools of 50-100 seedlings
773 treated in parallel. Asterisks denote significant differences as above (two-way ANOVA; specific
774 pairwise comparisons using Tukey's HSD correction).

775 SUPPLEMENTARY FIGURE LEGENDS

776 **Supplementary Figure 1. Germination of *Brassica tournefortii* seed treated with**
777 **karrikins**
778 **a**, Structures of KAR_1, KAR_2 and two enantiomers of GR24. **b**, Germination response of the
779 "Merridin" batch of *B. tournefortii* seed treated with KAR_1 and KAR_2 after three days. **c-d**,
780 Germination response of the "Perth" batch to KAR_1 (**c**) and KAR_2 (**d**). Data in Figure 1a are
781 derived from the data shown in **c**. **e-f**, Uptake of KAR_1 and KAR_2 by imbibed seed, as determined
782 by GC-MS. All error bars are mean ± SE of n = 3 batches of 75 seed (**b**-**d**) or 3 samples of 40 mg
783 (**e**) or 20 mg (**f**) seed as described in Methods.

784 **Supplementary Figure 2. Extended phylogeny of eu-KAI2 and D14 proteins in**
785 **angiosperms**
786 Maximum likelihood phylogeny of KAI2 and D14 homologues in the Brassicaceae and
787 monocots, based on nucleotide data. Node values represent bootstrap support from 100
788 replicates. A KAI2 sequence from *Selaginella moellendorffii* (SmKAI2a; Waters et al. 2015)
789 serves as an outgroup for the eu-KAI2 clade.

790 **Supplementary Figure 3. Alignment of Brassica KAI2 sequences**
791 Full length protein coding regions of *KAI2* homologues from four *Brassica* species (*Brassica*
792 *tournefortii*, *B. rapa*, *B. nigra* and *B. oleracea*) were translated from database nucleic acid
793 sequences and aligned to *Arabidopsis thaliana* KAI2 using MAFFT (Katoh et al, 2002)
794 implemented in Geneious R10 software (Biomatters Ltd). Amino acid residues are coloured
795 according to polarity: yellow, non-polar (G, A, V, L, I, F, W, M, P); green, polar & uncharged (S, T,
796 C, Y, N, Q); red, polar & acidic (D, E); blue, polar & basic (K, R, H). Residues that are unique to
797 BtKAI2c but otherwise invariant are highlighted with asterisks (*); residues 98 and 191 are
798 highlighted with red boxes.

799

800 **Supplementary Figure 4. BtD14a is functionally homologous to AtD14**
801 Three independent transgenic lines of Arabidopsis *Atd14-1* were analysed for functional
802 complementation of the mutant phenotype by an *AtD14pro:BtD14a* transgene. **a**, Rosette and
803 leaf morphology at 31 days post-germination. **b**, Plant height and number of primary rosette
804 branches at 45 days post-germination. **c**, Quantification of height and branching parameters, *n*
805 = 10 plants per genotype. Scale bars: 50 mm.

806 **Supplementary Figure 5. Expression of BtKAI2 homologues in Arabidopsis and tobacco**
807 **a**, Quantitative RT-PCR analysis of *GFP* and *DLK2* transcripts, normalised to *CACS* reference
808 transcripts. Data are derived from a single biological sample with four technical PCR replicates.
809 RNA was isolated from approximately 50 seven-day-old seedlings per genotype, and are the
810 same samples as those shown in the immunoblots in Figure 2d. **b**, Alignment of the protein
811 regions corresponding to the peptide epitope TTNPDYFDFDRYSN of AtKAI2, against which the
812 anti-KAI2 peptide was raised. BtKAI2b, with a more divergent epitope, is relatively poorly
813 detected by the anti-KAI2 antibody (see Figure 2d). **c**, Transient expression of BtKAI2a,
814 BtKAI2b and BtKAI2c proteins in tobacco. Plasmids encoding N-terminal, *c*-myc-tagged
815 proteins were transferred to *Agrobacterium*, and the resulting strains used to infiltrate tobacco
816 leaves. After 96 h, samples were harvested in triplicate (two to three leaves per sample). Mock-
817 treated leaves were transformed with a plasmid encoding a non-tagged protein. Sixty
818 micrograms of total protein were separated by SDS-PAGE, blotted and challenged with anti-*c*-
819 myc antibody (Genscript A00704). Band intensity was measured using ImageJ, and expression
820 was normalised to intensity of the Rubisco large subunit (RbcL) band on the "stain-free" gel
821 imaged under UV light. Error bars indicate SE, *n* = 3 replicates.

822 **Supplementary Figure 6. The GFP-BtKAI2c transgene is faithfully transcribed in**
823 **Arabidopsis**
824 **a**, Structure of the *AtKAI2pro:mGFP6-BtKAI2c* transgene. Primers used for RT-PCR are shown
825 with arrows. The promoter and 5′UTR are derived from *At4g37470* (*AtKAI2*). attB1, Gateway
826 recombination site that links *mGFP6* and *BtKAI2c* regions; *nos ter*, nopaline synthase
827 terminator. Not drawn to scale. **b**, RT-PCR analysis of *GFP-BtKAI2c* transcripts after 35 cycles
828 of amplification. Primers MW406 + BK010 target the transgene, while a second primer pair
829 (MW275 + MW278) serves as a control and spans five introns of *At1g03055*. *kai2-2* serves as a
830 non-transgenic control genotype. Templates: R, total RNA; D, genomic DNA; W, water only. RT,
831 reverse transcriptase (Supercript III). DNA size standards (in base pairs) are indicated on the
832 left, with anticipated PCR product sizes shown on the right and defined in the table. **c**, The RT-

833 PCR product generated with proof-reading polymerase (Q5, New Engalnd Biolabs) and primers
834 MW406 and BK010 was cloned into pCR4-TOPO (Life Technologies). Five dideoxy sequence
835 traces were aligned against the *GFP-BtKAI2c* transgene reference. No disagreements with the
836 reference sequence were observed. Red bars indicate trimmed regions of sequence traces to
837 remove low quality data.

838 **Supplementary Figure 7. Germination profiles of transgenic Arabidopsis seeds**
839 **expressing BtKAI2 homologues**
840 Freshly harvested seed (three batches per genotype, each batch harvested from four plants)
841 were removed from freezer storage, surface-sterilised and sown on 1% Phytagel supplemented
842 with 0.1% acetone (mock), 1 μM KAR_1 or 1 μM KAR_2. Seed were incubated under constant light
843 at 25 °C. Seed were examined for germination (radicle protrusion) 72 h after sowing and every
844 24 h thereafter. Data are means ± SE of three independent seed batches and 75 seed per batch.
845 For each transgene, two independent, homozygous transgenic lines were analysed. Data
846 presented in Figure 3 of the main manuscript are derived from these data.

847 **Supplementary Figure 8. SDS-PAGE of SUMO-BtKAI2 fusion proteins used for DSF**
848 To assess purity after affinity chromatography, five micrograms of each purified protein was
849 electrophoresed on a 12% acrylamide gel containing 2,2,2-trichloroethanol and visualised
850 under UV light. Protein size standards at 75 and 25 kDa (Bio-Rad Precision Plus Dual Colour)
851 fluoresce strongly under UV light.

852 **Supplementary Figure 9. BtKAI2a and BtKAI2b do not respond to karrikins in DSF assays**
853 Differential scanning fluorimetry curves of BtKAI2a and BtKAI2b in presence of 0–200 μM KAR_1
854 or KAR_2 (**a**) or the two enantiomers of GR24 (**b**). Data are means of eight technical replicates at
855 each concentration of ligand.

856 **Supplementary Figure 10. Stable transgenic expression of BtKAI2 valine–leucine**
857 **exchange proteins in Arabidopsis**
858 **a**, Immunoblots of total soluble protein extracted from 7-day-old seedlings of independent
859 transgenic lines segregating in a 3:1 ratio for hygromycin resistance. Transgene expression in
860 six lines expressing *GFP-BtKAI2a*$^{L98;L191}$ (upper panels) and five expressing *GFP-BtKAI2b*$^{V98;V191}$
861 (lower panels) were compared to a representative unmodified control (*GFP-BtKAI2a* 1F and
862 *GFP-BtKAI2b* 9A respectively). Based on expression level two lines of each construct (3-5 and
863 3-14; 6-4 and 6-13) were selected and brought to homozygosity for further experiments.
864 Protein blots were challenged with anti-GFP antibody. Equal gel loading was assessed by

865 imaging total protein prior to blotting; the RbcL band is shown. **b**, Rosette phenotypes of
866 homozygous individuals expressing native and modified *GFP-BtKAI2* transgenes. Plants were
867 25 days old and grown under long day conditions as described in Methods. Scale bar: 50 mm.

868 **Supplementary Figure 11. Three experimental replicates of hypocotyl elongation assays**
869 **with BtKAI2 Arabidopsis transgenics**
870 Each panel depicts data from an independent experiment performed on a separate date, which
871 are shown in summarised format in Figure 5. Data are means ± SE, n=24 to 40 seedlings. Each
872 dot corresponds to an individual seedling.

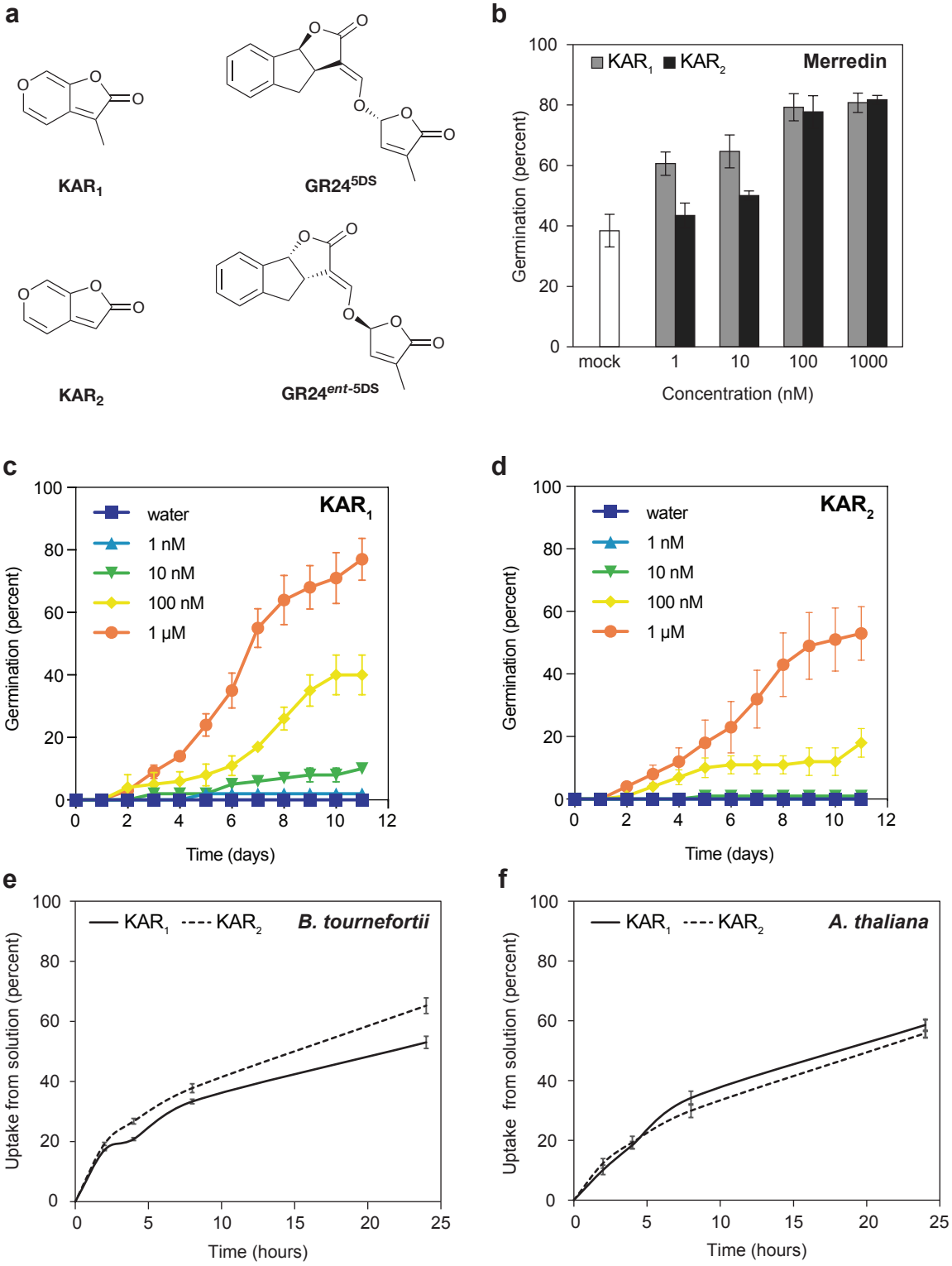

Supplementary Figure 1. Germination of *Brassica tournefortii* seed treated with karrikins
a, Structures of KAR_1, KAR_2 and two enantiomers of GR24. **b,** Germination response of the "Merridin" batch of *B. tournefortii* seed treated with KAR_1 and KAR_2 after three days. **c-d,** Germination response of the "Perth" batch to KAR_1 (**c**) and KAR_2 (**d**). Data in Figure 1a are derived from the data shown in **c.** **e-f**, Rates of KAR_1 and KAR_2 uptake by imbibed seed, as determined by GC-MS. All error bars are mean ± SE of n = 3 batches of 75 seed (b-d) or 3 samples of 40 mg (e) or 20 mg (f) seed as described in Methods.

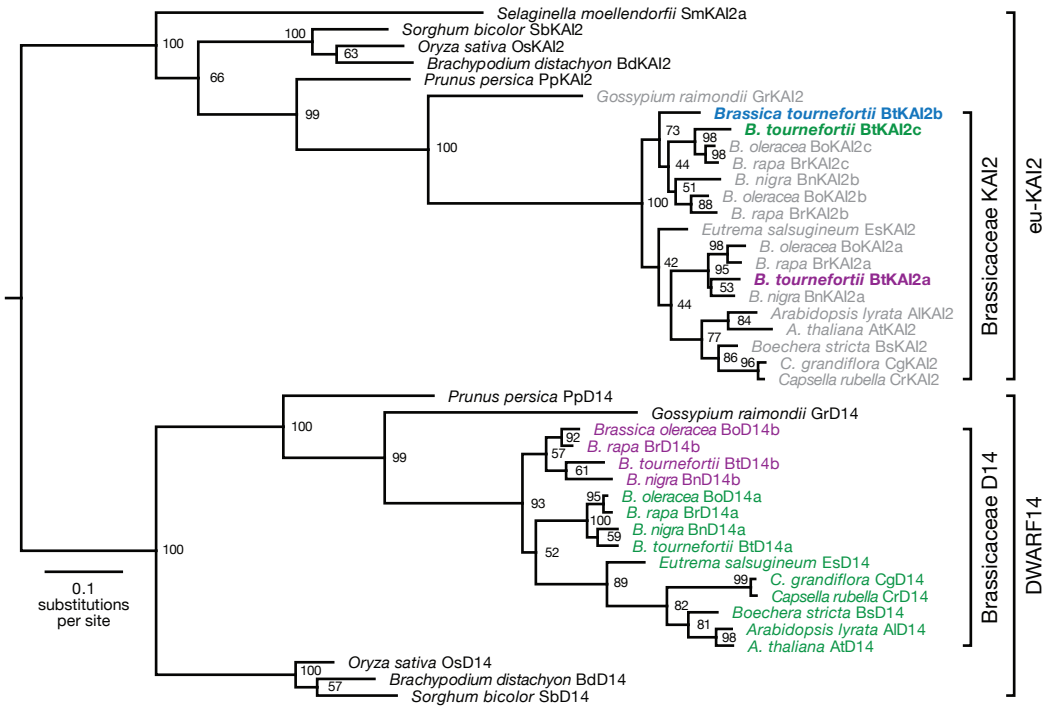

Supplementary Figure 2. Extended phylogeny of eu-KAI2 and D14 proteins in angiosperms
Maximum likelihood phylogeny of KAI2 and D14 homologues in the Brassicaceae and monocots, based on nucleotide data. Node values represent bootstrap support from 100 replicates. A KAI2 sequence from *Selaginella moellendorffii* (SmKAI2a; Waters et al. 2015) serves as an outgroup for the eu-KAI2 clade.

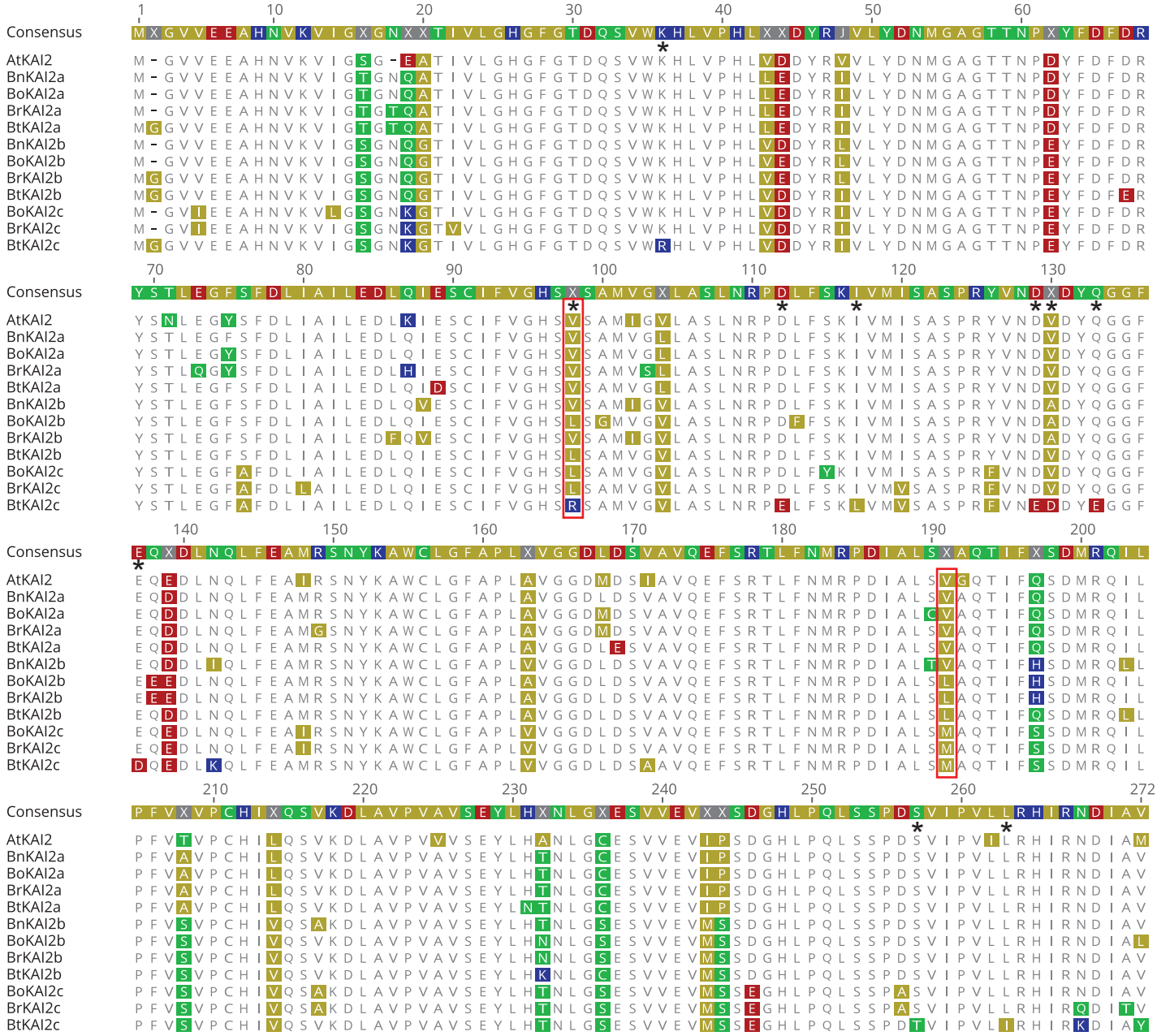

Supplementary Figure 3. Alignment of *Brassica* KAI2 sequences

Full length protein coding regions of KAI2 homologues from four *Brassica* species (*Brassica tournefortii*, *B. rapa*, *B. nigra* and *B. oleracea*) were translated from database nucleic acid sequences and aligned to Arabidopsis KAI2 using MAFFT (Katoh et al, 2002) implemented in Geneious R10 software (Biomatters Ltd). Amino acid residues are coloured according to polarity: yellow, non-polar (G, A, V, L, I, F, W, M, P); green, polar & uncharged (S, T, C, Y, N, Q); red, polar & acidic (D, E); blue, polar & basic (K, R, H). Residues that are unique to BtKAI2c but otherwise invariant are highlighted with asterisks (*); residues 98 and 191 are highlighted with red boxes.

Supplementary Figure 4. BtD14a is functionally homologous to AtD14
Three independent transgenic lines of Arabidopsis *Atd14-1* were analysed for functional complementation of the mutant phenotype by an *AtD14pro:BtD14a* transgene. **a**, Rosette and leaf morphology at 31 days post-germination. **b**, Plant height and number of primary rosette branches at 45 days post-germination. **c**, Quantification of height and branching parameters, means ± SE, *n* = 10 plants per genotype. Scale bars: 50 mm.

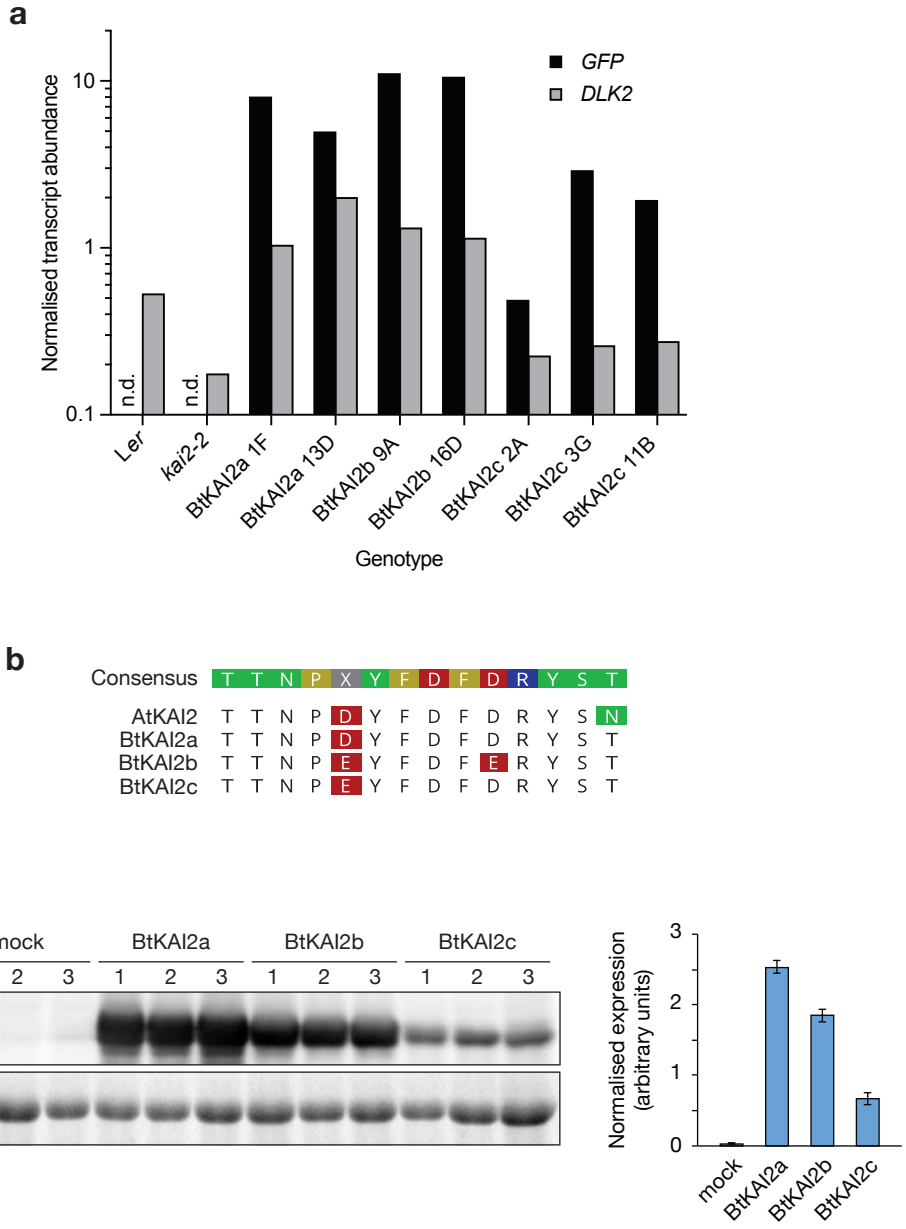

Supplementary Figure 5. Expression of BtKAI2 homologues in Arabidopsis and tobacco
a, Quantitative RT-PCR analysis of *GFP* and *DLK2* transcripts, normalised to *CACS* reference transcripts. Data are derived from a single biological sample with four technical PCR replicates. RNA was isolated from approximately 50 seven-day-old seedlings per genotype, and are the same samples as those shown in the immunoblots in Figure 2. **b**, Alignment of the protein regions corresponding to the peptide epitope TTNPDYFDFDRYSN of AtKAI2, against which the anti-KAI2 peptide was raised. BtKAI2b, with a more divergent epitope, is relatively poorly detected by the anti-KAI2 antibody (see Figure 2). **c**, Transient expression of BtKAI2a, BtKAI2b and BtKAI2c proteins in tobacco. Plasmids encoding N-terminal, c-myc-tagged proteins were transferred to Agrobacterium, and the resulting strains used to infiltrate tobacco leaves. After 96 h, samples were harvested in triplicate (two to three leaves per sample). Mock-treated leaves were transformed with a plasmid encoding a non-tagged protein. Sixty micrograms of total protein were separated by SDS-PAGE, blotted and challenged with anti-c-myc antibody (Genscript A00704). Band intensity was measured using ImageJ, and expression was normalised to intensity of the Rubisco large subunit (RbcL) band on the “stain-free” gel imaged under UV light. Error bars indicate SE, n = 3 replicates.

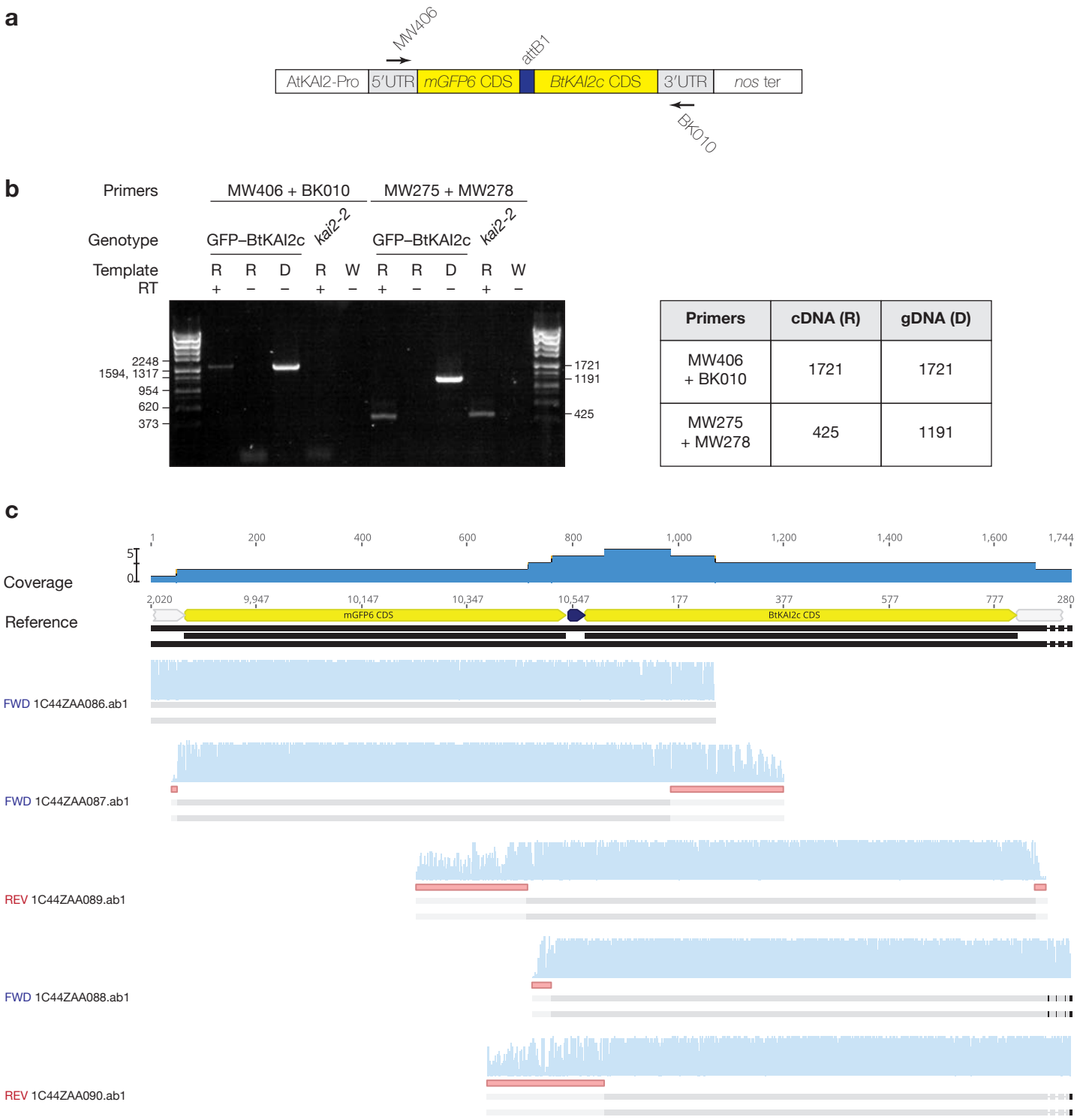

Primers	cDNA (R)	gDNA (D)
MW406 + BK010	1721	1721
MW275 + MW278	425	1191

Supplementary Figure 6. The *GFP-BtKAI2c* transgene is faithfully transcribed in Arabidopsis

a, Structure of the *AtKAI2pro:mGFP6-BtKAI2c* transgene. Primers used for RT-PCR are shown with arrows. The promoter and 5′UTR are derived from *At4g37470* (*AtKAI2*). attB1, Gateway recombination site that links mGFP6 and BtKAI2c regions; *nos* ter, nopaline synthase terminator. Not drawn to scale.

b, RT-PCR analysis of *GFP-BtKAI2c* transcripts after 35 cycles of amplification. Primers MW406 + BK010 target the transgene, while a second primer pair (MW275 + MW278) serves as a control and spans five introns of *At1g03055*. *kai2-2* serves as a non-transgenic control genotype. Templates: R, total RNA; D, genomic DNA; W, water only. RT, reverse transcriptase (Supercript III). DNA size standards (in base pairs) are indicated on the left, with anticipated PCR product sizes shown on the right and defined in the table.

c, The RT-PCR product generated with proof-reading polymerase (Q5, New Engalnd Biolabs) and primers MW406 and BK010 was cloned into pCR4-TOPO (Life Technologies). Five dideoxy sequence traces were aligned against the *GFP-BtKAI2c* transgene reference. No disagreements with the reference sequence were observed. Red bars indicate trimmed regions of sequence traces to remove low quality data.

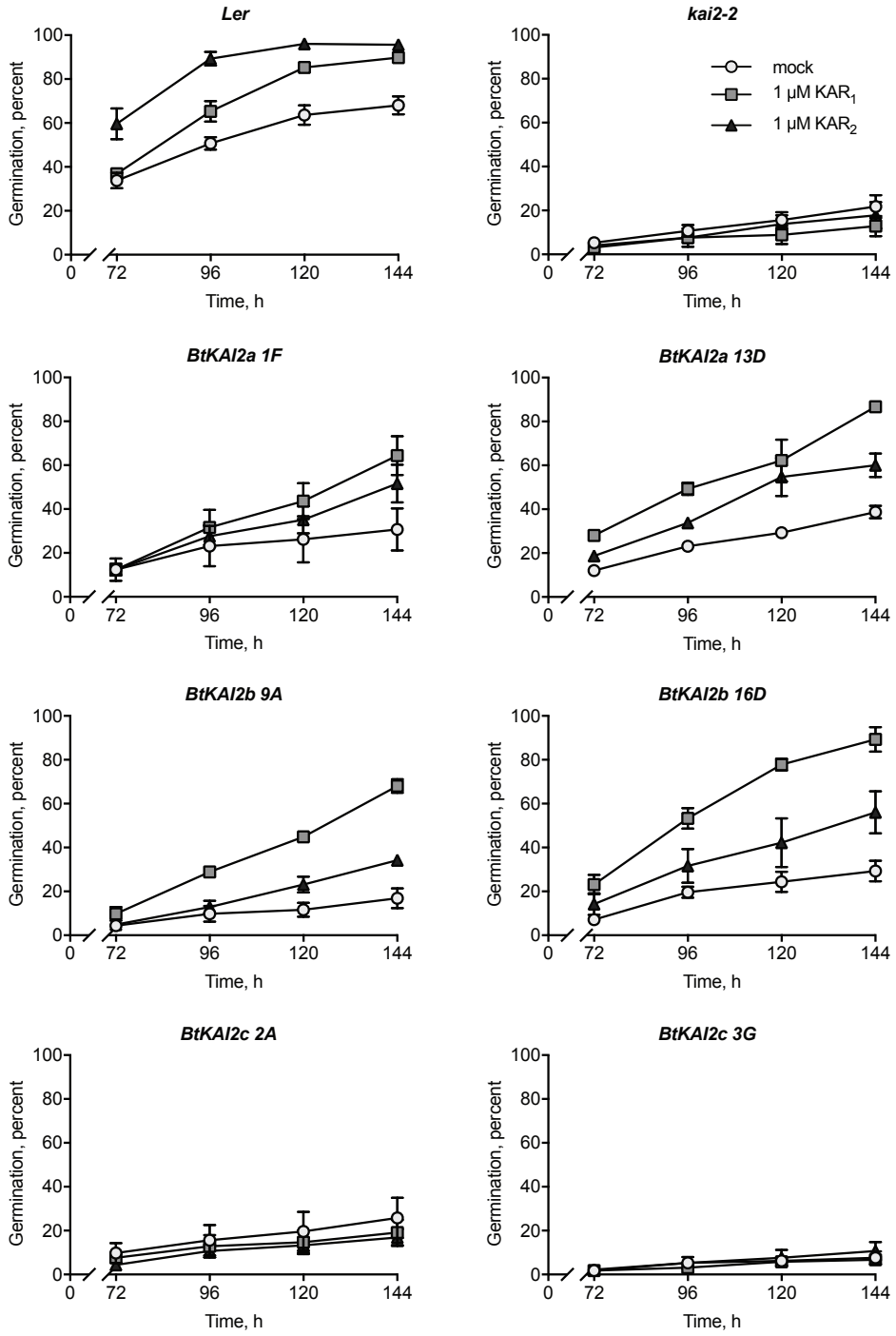

Supplementary Figure 7. Germination profiles of transgenic Arabidopsis seeds expressing BtKAI2 homologues
Freshly harvested seed (three batches per genotype, each batch harvested from four plants) were removed from freezer storage, surface-sterilised and sown on 1% Phytagel supplemented with 0.1% acetone (mock), 1 μM KAR_1 or 1 μM KAR_2. Seed were incubated under constant light at 25 °C. Seed were examined for germination (radicle protrusion) 72 h after sowing and every 24 h thereafter. Data are means ± SE of three independent seed batches and 75 seed per batch. For each transgene, two independent, homozygous transgenic lines were analysed. Data presented in Figure 3 of the main manuscript are derived from these data.

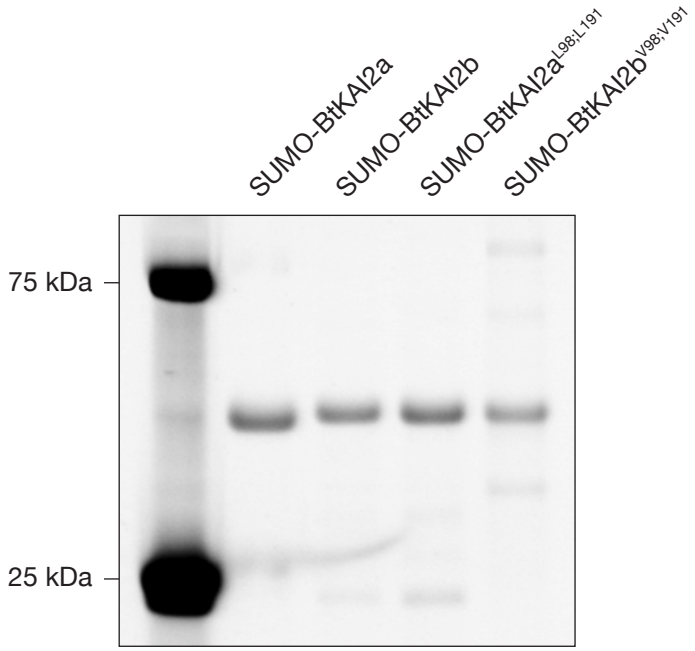

Supplementary Figure 8. SDS-PAGE of SUMO-BtKAI2 fusion proteins used for DSF.
To assess purity after affinity chromatography, five micrograms of each purified protein was electrophoresed on a 12% acrylamide gel containing 2,2,2-trichloroethanol and visualised under UV light. Protein size standards at 75 and 25 kDa (Bio-Rad Precision Plus Dual Colour) fluoresce strongly under UV light.

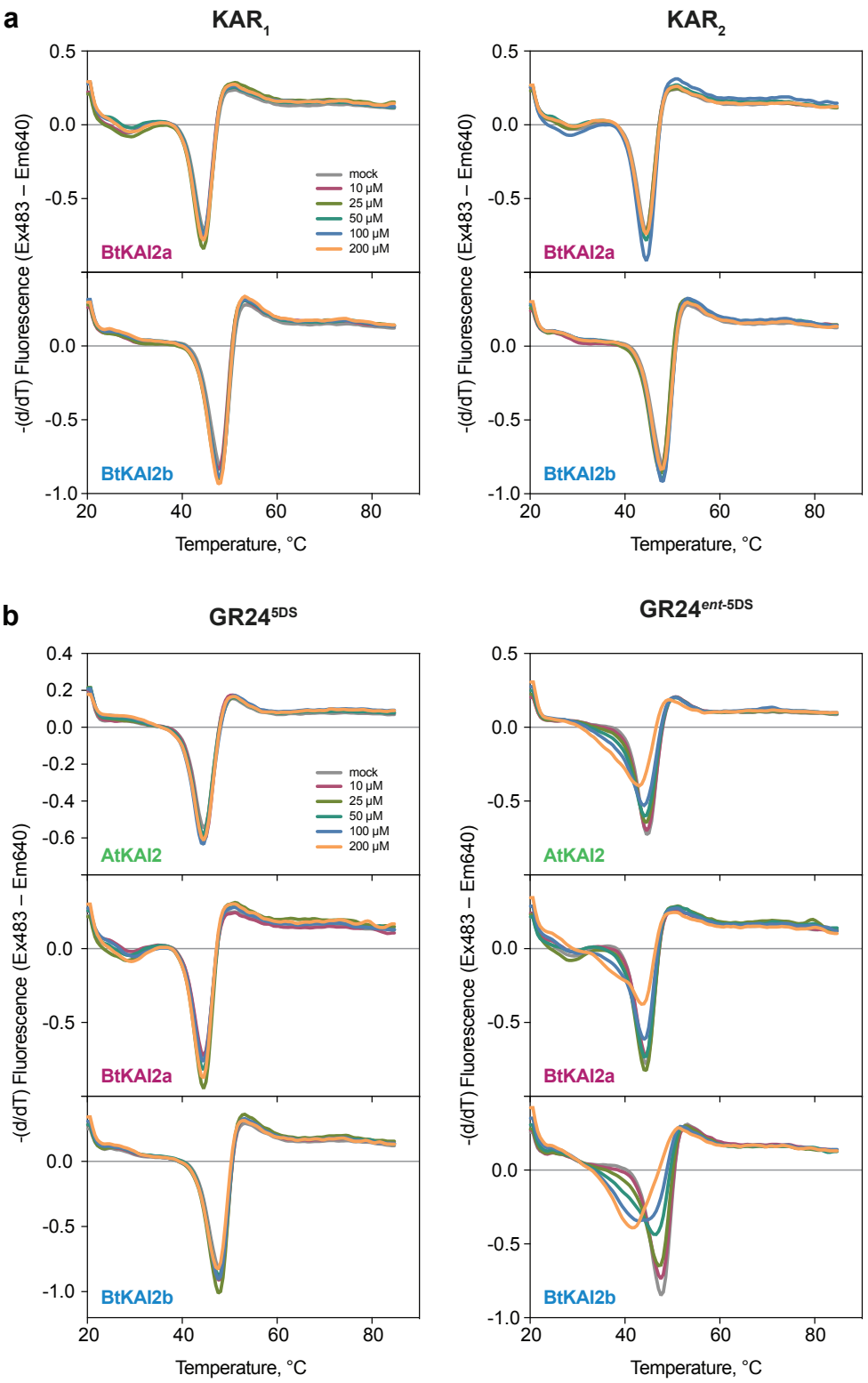

Supplementary Figure 9. BtKAI2a and BtKAI2b do not respond to karrikins in DSF assays
Differential scanning fluorimetry curves of SUMO-BtKAI2a and SUMO-BtKAI2b in presence of 0–200 µM KAR_1 or KAR_2 (**a**) or the two enantiomers of GR24 (**b**). Data are means of eight technical replicates at each concentration of ligand.

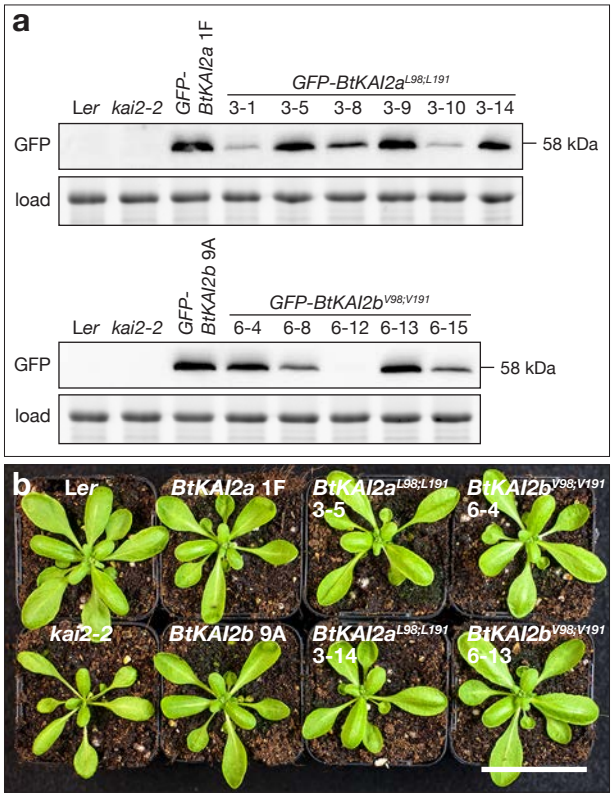

Supplementary Figure 10. Stable transgenic expression of BtKAI2 valine–leucine exchange proteins in Arabidopsis

a, Immunoblots of total soluble protein extracted from 7-day-old seedlings of independent transgenic lines segregating in a 3:1 ratio for hygromycin resistance. Transgene expression in six lines expressing GFP-BtKAI2a$^{L98;L191}$ (upper panels) and five expressing GFP-BtKAI2b$^{V98;V191}$ (lower panels) were compared to a representative unmodified control (GFP-BtKAI2a 1F and GFP-BtKAI2b 9A respectively). Based on expression level two lines of each construct (3-5 and 3-14; 6-4 and 6-13) were selected and brought to homozygosity for further experiments. Protein blots were challenged with anti-GFP antibody. Equal gel loading was assessed by imaging total protein prior to blotting; the RbcL band is shown. **b**, Rosette phenotypes of homozygous individuals expressing native and modified *GFP-BtKAI2* transgenes. Plants were 25 days old and grown under long day conditions as described in Methods. Scale bar: 50 mm.

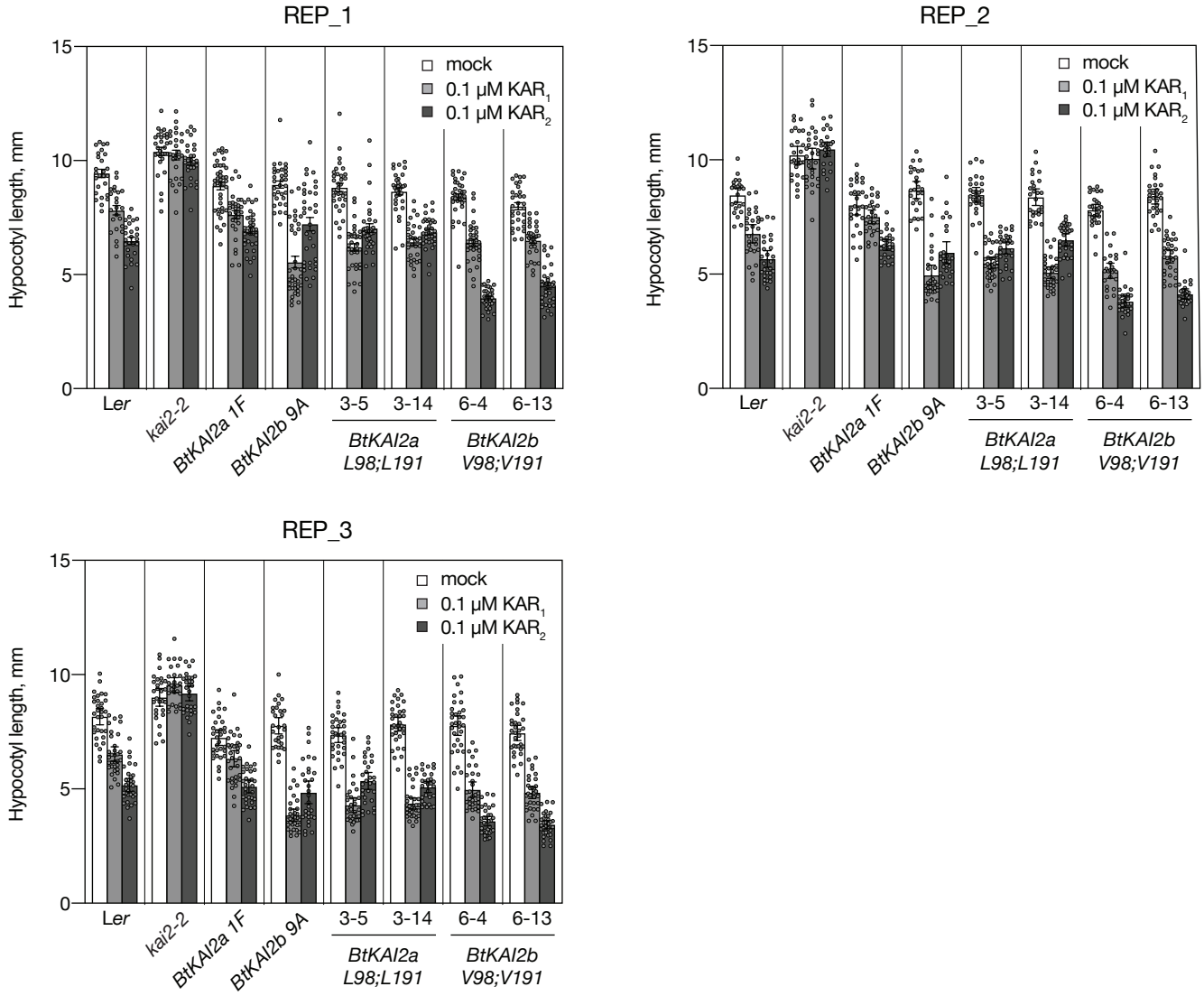

Supplemental Figure 11. Three experimental replicates of hypocotyl elongation assays with BtKAI2 Arabidopsis-transgenics

Each panel depicts data from an independent experiment performed on a separate date, which are shown in summarised format in Figure 5. Data are means ± SE, n=24 to 40 seedlings. Each dot corresponds to an individual seedling.

Supplementary Table 1. List of sequences identified in this study

KAI2

Species	Gene name	Sequence ID	Source	Reference
Arabidopsis lyrata	*AlKAI2*	AL7G13320.t1	Phytozome	This work
Arabidopsis thaliana	*AtKAI2*	At3g37470	TAIR	Waters et al (2012)
Brassica tournefortii (saharan mustard)	*BtKAI2a*	MG783328	GenBank/NCBI	This work
Brassica tournefortii (saharan mustard)	*BtKAI2b*	MG783329	GenBank/NCBI	This work
Brassica tournefortii (saharan mustard)	*BtKAI2c*	MG783330	GenBank/NCBI	This work
Brassica rapa (field mustard, AA genome)	*BrKAI2a*	XM_009111126.2	GenBank/NCBI	This work
Brassica rapa (field mustard, AA genome)	*BrKAI2b*	XM_009140247	GenBank/NCBI	This work
Brassica rapa (field mustard, AA genome)	*BrKAI2c*	XM_009144693	GenBank/NCBI	This work
Brassica nigra (black mustard, BB genome)	*BnKAI2a*	LFLV01000699.1	GenBank/NCBI	This work
Brassica nigra (black mustard, BB genome)	*BnKAI2b*	LFLV01001772.1	GenBank/NCBI	This work
Brassica oleracea (cabbage, CC genome)	*BoKAI2a*	XM_013766720.1	Phytozome	This work
Brassica oleracea (cabbage, CC genome)	*BoKAI2b*	XM_013738288.1	Phytozome	This work
Brassica oleracea (cabbage, CC genome)	*BoKAI2c*	XM_013778816.1	Phytozome	This work
Boechera stricta	*BsKAI2*	Bostr.30440s0001.1	Phytozome	This work
Capsella rubella	*CrKAI2*	Carubv10005485m	Phytozome	This work
Capsella grandiflora	*CgKAI2*	Cagra.1232s0005.1	Phytozome	This work
Eutrema salsugineum	*EsKAI2*	Thalv10025969m	Phytozome	Bythell-Douglas et al (2017)
Gossypium raymondii	*GrKAI2*	Gorai.003G028500.1	Phytozome	Bythell-Douglas et al (2017)
Prunus persica	*PpKAI2*	Ppa009957m	Phytozome	Bythell-Douglas et al (2017)
Brachypodium distachyon	*BdKAI2*	Bradi1g15880.1	Phytozome	Bythell-Douglas et al (2017)
Oryza sativa	*OsKAI2*	Os03g32270.1	Phytozome	Bythell-Douglas et al (2017)
Sorghum bicolor	*SbKAI2*	Sorbic.001G330000.1	Phytozome	Bythell-Douglas et al (2017)
Selaginella moellendorffii	*SmKAI2a*	Selmo_441991	Phytozome	Waters et al (2015)

D14

Species	Gene name	Sequence ID	Source	Reference
Arabidopsis lyrata	*AlD14*	AL3G13900.t1	Phytozome	This work
Arabidopsis thaliana	*AtD14*	AT3G03990.1	TAIR	Waters et al (2012)
Brassica oleracea (cabbage, CC genome)	*BoD14a*	LOC106343216	Phytozome	This work
Brassica oleracea (cabbage, CC genome)	*BoD14b*	LOC106343689	Phytozome	This work
Brassica nigra (black mustard, BB genome)	*BnD14a*	LFLV01002090	GenBank/NCBI	This work
Brassica nigra (black mustard, BB genome)	*BnD14b*	LFLV01000699	GenBank/NCBI	This work
Brassica rapa (field mustard, AA genome)	*BrD14a*	Brara.A03790	Phytozome	This work
Brassica rapa (field mustard, AA genome)	*BrD14b*	Brara.E03476	Phytozome	This work
B. tournefortii (saharan mustard)	*BtD14a*	MG783331	Phytozome	This work
B. tournefortii (saharan mustard)	*BtD14b*	MG783332	Phytozome	This work
Boechera stricta	*BsD14*	Bostr.2570s0310	Phytozome	This work
Capsella grandiflora	*CgD14*	Cagra.15970s0001	Phytozome	This work
Capsella rubella	*CrD14*	Carubv10014401m	Phytozome	This work
Eutrema salsugineum	*EsD14*	Thhalv10021292m	Phytozome	Bythell-Douglas et al (2017)
Gossypium raymondii	*GrD14*	Gorai.010G025600.1	Phytozome	Bythell-Douglas et al (2017)
Prunus persica	*PpD14*	ppa010005m	Phytozome	Bythell-Douglas et al (2017)
Brachypodium distachyon	*BdD14*	Bradi1g70930.3	Phytozome	Bythell-Douglas et al (2017)
Oryza sativa	*OsD14*	Os03g10620.1	Phytozome	Bythell-Douglas et al (2017)
Sorghum bicolor	*SbD14*	Sobic.001G465100.1	Phytozome	Bythell-Douglas et al (2017)

DLK2

Species	Gene name	Sequence ID	Source	Reference
B. tournefortii (saharan mustard)	*BtDLK2*	MG783333	GenBank/NCBI	This work

Supplementary Table 2. Oligonucleotides used in this study

Oligonucleotide	Sequence	Notes
Cloning		
BtD14a_F	AAAAAAGCAGGCTTCCATTATGAGTCAACACAACAT	BtD14a
BtD14a_R	CAAGAAAGCTGGGTTTTAAAGTCACCGAGGAAG	BtD14a
BtKAI2_universal_F	GGGGACAAGTTTGTACAAAAAAGCAGGCTTCATGGGAGGTGTGGTAGAGGA	All BtKAI2
RACE_R	GGGGACCACTTTGTACAAGAAAGCTGGGTCATTCTCAATAGACAATAGAC	BtKAI2a
Contig1_R	GGGGACCACTTTGTACAAGAAAGCTGGGTCCGAAACGACCCACTCACTTACC	BtKAI2b
Contig5_R	GGGGACCACTTTGTACAAGAAAGCTGGGTCCGAAGCAGAACCAAGCTAA	BtKAI2c
BtKAI2-SUMO-Gib_F	TGAGGCTCACCGCGAACAGATTGGAGGTATGGGAGGTGTGGTAGAGGAAG	pSUMO-BtKAI2a / BtKAI2b
BtKAI2a-SUMO-Gib_R	CGGATCTCAGTGGTGGTGGTGGTGGTGCTCAGACAGCGATGTCATTACGA	pSUMO-BtKAI2a
BtKAI2b-SUMO-Gib_R	CGGATCTCAGTGGTGGTGGTGGTGGTGCTCATACAGCAATGTCGTTGCGG	pSUMO-BtKAI2b
BtKAI2b_L98V_F1	ATCTTTGTTGGTCACTCTGTCTCCGCCATG	For BtKAI2b(a) mutagenesis
BtKAI2b_L191V_R1	TTTGGAAAATGGTCTGAGCCACGGAGAGTG	For BtKAI2b(a) mutagenesis
BtKAI2b_L191V_F2	TCTCCGTGGCTCAGACCATTTTCCAAAGC	For BtKAI2b(a) mutagenesis
BtKAI2b_L98V_R2	CATGGCGGAGACAGAGTGACCAACAAAG	For BtKAI2b(a) mutagenesis
BtKAI2a_V98L_F1	ATCTTTGTTGGTCACTCTCTCTCCGCCATG	For BtKAI2a(b) mutagenesis
BtKAI2a_V191L_R1	TTTGGAAAATGGTCTGAGCCAGGGAGAGAG	For BtKAI2a(b) mutagenesis
BtKAI2a_V191L_F2	TCTCCCTGGCTCAGACCATTTTCCAAAG	For BtKAI2a(b) mutagenesis
BtKAI2a_V98L_R2	CATGGCGGAGAGAGAGTGACCAACAAAG	For BtKAI2a(b) mutagenesis
MW406	CACGAACTGACTAAGAGAGG	For cloning GFP-BtKAI2c cDNA
BK010	GAAACGATATACTCAGTACTTACCAC	For cloning GFP-BtKAI2c cDNA
Quantitative PCR		
BtSTH7_qF	CATCTCCGGTTCTCTCTCACTTCT	Designed against At4g39070
BtSTH7_qR	CATTCTCTGCATAGTATTGCTCTGTC	Designed against At4g39070
BtDLK2_qF	GCTGCTTCTCCCAGGTATATAA	BtDLK2
BtDLK2_qR	GAAAGCAACCGCCCAAGCC	BtDLK2
AtDLK2_qF	GCTGCTTCTCCAAGGTATATAA	Designed against At3g24420
AtDLK2_qR	GAAATCAACCGCCCAAGCT	Designed against At3g24420
BtKAI2_universal_qF	GGTCATCTTCCTCAGCTTAG	All BtKAI2
BtKAI2_a_qR1	CCATTAATTTAATTTAAAATCACTTCCC	BtKAI2a
BtKAI2_b_qR1	GCATTTAATTTCGCTAAAACTCTTG	BtKAI2b
BtKAI2_c_qR1	GAAACGATATACTCAGTACTTACCAC	BtKAI2c
CACS_qF	ACTCAGGAAGGTGTACGGTCA	Designed against At5g46630
CACS_qR	TGCATTTGGAACAGGTTTGT	Designed against At5g46630
BtCACS_qF	ACTCAGGAAGGTGTACGGTCA	Designed against At5g46630
BtCACS_qR	TGCATTTGGAACAGGTTTGT	Designed against At5g46630